NORSAR

ROYAL NORWEGIAN COUNCIL FOR SCIENTIFIC AND INDUSTRIAL RESEARCH

Scientific Report No. 1-84/85

SEMIANNUAL TECHNICAL SUMMARY

1 April – 30 September 1984

Linda B. Loughran (Ed.)

Kjeller, November 1984

UNCLASSIFIED

SECURITY CLASSIFICATION OF THIS PAGE

REPORT DOCUMENTATION PAGE

1a. REPORT SECURITY CLASSIFICATION UNCLASSIFIED	1b. RESTRICTIVE MARKINGS NOT APPLICABLE
2a. SECURITY CLASSIFICATION AUTHORITY NOT APPLICABLE	3. DISTRIBUTION/AVAILABILITY OF REPORT APPROVED FOR PUBLIC RELEASE DISTRIBUTION UNLIMITED
2b. DECLASSIFICATION/DOWNGRADING SCHEDULE NOT APPLICABLE	
4. PERFORMING ORGANIZATION REPORT NUMBER(S) SCIENTIFIC REPORT 1-84/85	5. MONITORING ORGANIZATION REPORT NUMBER(S) SCIENTIFIC REPORT 1-84/85
6a. NAME OF PERFORMING ORGANIZATION NTNF/NORSAR 6b. OFFICE SYMBOL (If applicable)	7a. NAME OF MONITORING ORGANIZATION HQ AFTAC/TGX
6c. ADDRESS (City, State and ZIP Code) POST BOX 51 N-2007 KJELLER, NORWAY	7b. ADDRESS (City, State and ZIP Code) PATRICK AFB, FL 32925-6471
8a. NAME OF FUNDING/SPONSORING ORGANIZATION DEFENSE ADVANCED RESEARCH PROJECTS AGENCY 8b. OFFICE SYMBOL (If applicable)	9. PROCUREMENT INSTRUMENT IDENTIFICATION NUMBER CONTRACT NO. F08606-84-C-0002
8c. ADDRESS (City, State and ZIP Code) ARLINGTON, VA 22209	10. SOURCE OF FUNDING NOS. PROGRAM ELEMENT NO.: R&D PROJECT NO.: NORSAR PHASE 3 TASK NO.: SOW TASK 5.0 WORK UNIT NO.: SEQUENCE NUMBER 003A2
11. TITLE (Include Security Classification) SEMIANNUAL TECHNICAL SUMMARY 1 APR-30 SEP 84 (UNCLASSIFIED)	
12. PERSONAL AUTHOR(S) L.B. LOUGHRAN (ED.)	
13a. TYPE OF REPORT SCIENTIFIC SUMMARY 13b. TIME COVERED FROM 1 APR TO 30 SEP	14. DATE OF REPORT (Yr., Mo., Day) 84 15. PAGE COUNT
16. SUPPLEMENTARY NOTATION NOT APPLICABLE	

17. COSATI CODES			18. SUBJECT TERMS (Continue on reverse if necessary and identify by block number)
FIELD	GROUP	SUB. GR.	NORSAR, NORWEGIAN SEISMIC ARRAY

19. ABSTRACT (Continue on reverse if necessary and identify by block number)

The Norwegian Seismic Array (NORSAR) Detection Processing System has been operated through the period 1 April - 30 September 1984 with an average up time of 95.1 per cent. Most of the down time has been caused by MODCOMP computer problems. A total of 2160 seismic events have been reported by NORSAR in the period. A new alarm system has been installed to alert the operator on duty in case of system problems. A new telex connection has been established to provided automatic bulletin transmission to AFTAC three times a day, seven days a week.

A seismic waveform inversion technique has been developed and applied to deep events in the Fiji Islands region. Preliminary results show no compelling evidence for significant deviations from the double couple mechanism; and the data are consistent with a stress drop in the range 10-100 bars. A new method for dynamic ray tracing

20. DISTRIBUTION/AVAILABILITY OF ABSTRACT UNCLASSIFIED/UNLIMITED ☒ SAME AS RPT. ☐ DTIC USERS ☐	21. ABSTRACT SECURITY CLASSIFICATION UNCLASSIFIED	
22a. NAME OF RESPONSIBLE INDIVIDUAL CAPT JAMES A. ROBB	22b. TELEPHONE NUMBER (Include Area Code) (305) 494-7665	22c. OFFICE SYMBOL AFTAC/TGX

DD FORM 1473, 83 APR EDITION OF 1 JAN 73 IS OBSOLETE.

UNCLASSIFIED

SECURITY CLASSIFICATION OF THIS PAGE

19. (cont'd)

is being developed, and has been tested against simple analytical models. An investigation of optimum data processing schemes for regional arrays has shown the need for operating over a relatively wide band of frequencies (2-8 Hz) in order to ensure adequate SNR for various signal paths (oceanic, mobile cratonic belt, shield). SNR gains of 2-4 dB (up to about 5 Hz) relative to conventional beamforming can be obtained using optimum weighting, whereas a simplified scheme of 0/1 weighting gives 1-2 dB less gain. An investigation of high-frequency P-wave attenuation from Central Asia to Norway has shown that for recordings of Semipalatinsk explosions there are almost no frequency-dependent effects in the attenuation between 3 and 7 Hz, thus confirming the assumption that the source spectrum of such events is proportional to f^{-2} above the corner frequency. An investigation of teleseismic detection at high frequencies at NORSAR has shown that significant gains (5-10 dB) relative to current performance can be obtained using several narrow-band high-frequency filters in the detection processor. A preliminary evaluation of the processing system for the planned NORESS array has shown that the success of the location part of the algorithm depends on a proper identification of secondary arrivals, and thus must take into account regionally dependent effects such as the apparent Lg "barrier" in the Viking Graben of the North Sea.

AFTAC Project Authorization	:	T/4141/B/PMP
ARPA Order No.	:	1483
Program Code No.	:	0F10
Name of Contractor	:	Royal Norwegian Council for Scientific and Industrial Research
Effective Date of Contract	:	1 October 1983
Contract Expiration Date	:	30 September 1984
Project Manager	:	Frode Ringdal (01) 71 69 15
Title of Work	:	The Norwegian Seismic Array (NORSAR) Phase 3
Amount of Contract	:	$ 796 000
Contract Period Covered by the Report	:	1 April - 30 September 1984

This research was supported by the Advanced Research Projects Agency of the Department of Defense and was monitored by AFTAC, Patrick AFB, FL 32925, under contract no. F08606-84-C-0002.

NORSAR Contribution No. 350

TABLE OF CONTENTS

I. SUMMARY

This report describes the operation, maintenance and research activities at the Norwegian Seismic Array (NORSAR) for the period 1 April - 30 September 1984.

The uptime of the NORSAR online detection processor system has averaged 95.1 per cent as compared to 95.6 for the previous period. Almost half the downtime came in July and was caused by power supply failure on the MODCOMP computer. A total of 2160 events were reported in this period, giving a daily average of 11.8 events. Frequent tests and interruptions of communications systems for 02C and 03C resulted in high error figures during week 15. These tests were connected with the malfunction in the MODCOMP computer, caused by a move in connection with a reorganization of the computer hall.

As a result of unsatisfactory performance of the old alarm system, a new alarm has been installed in the computer room. The new system has resulted in safer reporting of breakdowns in the online system and will hopefully result in an improved uptime. A new telex connection has been established enabling an automatic transmission of bulletin data to AFTAC 3 times a day, 7 days a week.

Section V describes maintenance activities in the field and at the NORSAR Maintenance Center.

The research activity is briefly described in section VII. Section VII.1 discusses source solutions from long-period waveform inversion. Section VII.2 presents a study on path effects and long-period station residuals in the GDSN network. Section VII.3 presents a preliminary report on a method of dynamic ray tracing, while VII.4 describes regional arrays and optimum data processing schemes. Section VII.5 takes up high-frequency P wave attenuation from Central Asia to Norway. In Section VII.6 some initial results are summarized with regard to possible improvements in NORSAR on-line event detection performance. Section VII.7 contains a review of recent developments concerning the new NORESS small-aperture array.

II. OPERATION OF ALL SYSTEMS

II.1 Detection Processor (DP) Operation

There have been 126 breaks in the otherwise continuous operation of the NORSAR online system within the current 6-month reporting interval. Almost half the downtime came in July and was caused by power trouble on the MODCOMP computer. The uptime percentage for the period is 95.1 as compared to 95.6 for the previous period.

Fig. II.1.1 and the accompanying Table II.1.1 both show the daily DP downtime for the days between 1 April and 30 September 1984. The monthly recording times and percentages are given in Table II.1.2.

The breaks can be grouped as follows:

a)	MODCOMP failure	47
b)	Stops related to program work or error	8
c)	Maintenance stops	8
d)	Power jumps and breaks	5
e)	Stops related to system operation	2
f)	TOD error correction	39
g)	Communication lines	17

The total downtime for the period was 215 hours and 1 minute. The mean-time-between-failures (MTBF) was 1.4 days, the same as for the previous period.

J. Torstveit

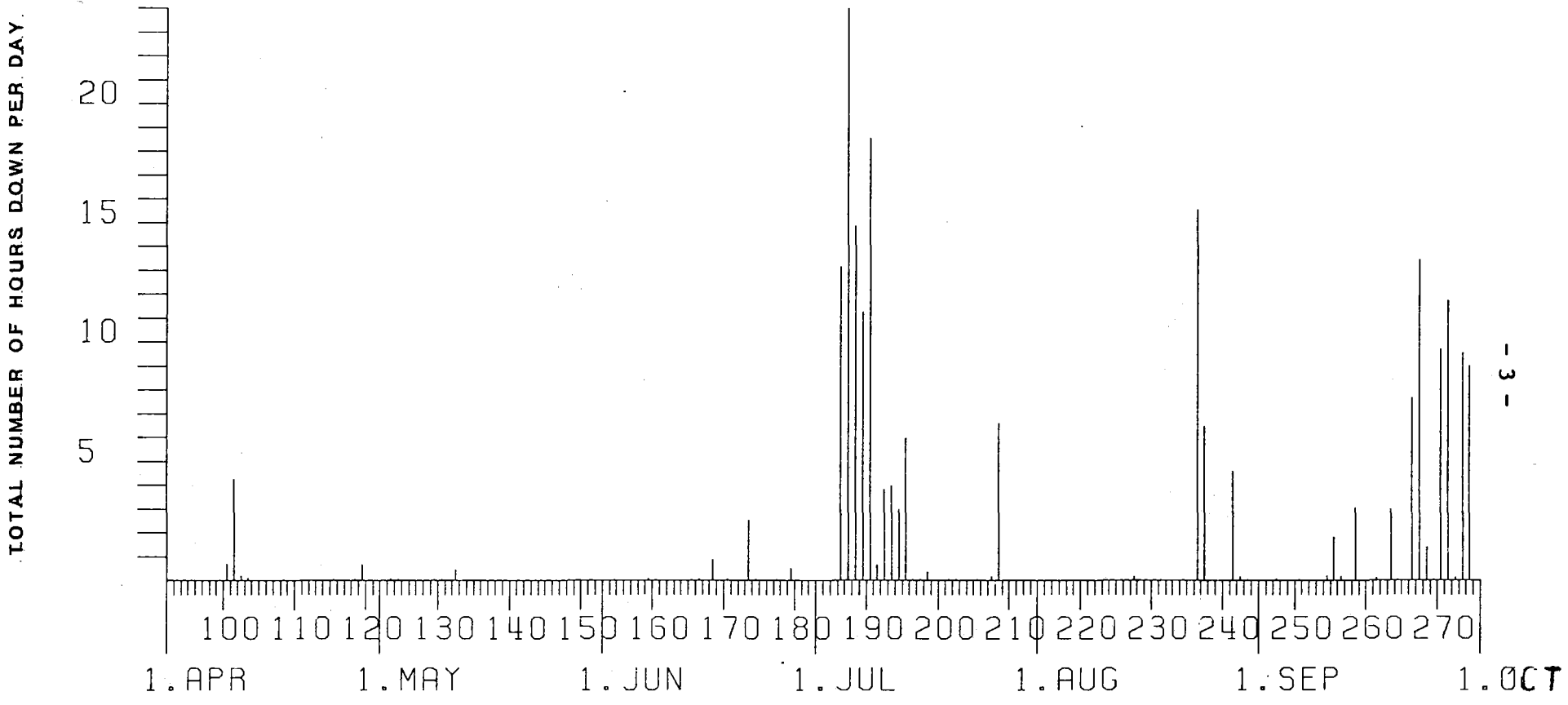

Fig. II.1.1 Detection Processor downtime in the period 1 April - 30 September 1984.

LIST OF BREAKS IN DP PROCESSING THE LAST HALF-YEAR

DAY	START		STOP		COMMENTS.....
94	5	47	5	49	TOD CORRECTION
100	6	14	6	15	MODCOMP FAILURE
100	7	28	8	7	POWER FAILURE
101	6	2	6	3	TOD CORRECTION
101	7	1	8	9	MODCOMP FAILURE
101	9	33	10	4	MODCOMP FAILURE
101	10	11	10	52	MODCOMP FAILURE
101	12	24	12	42	MODCOMP FAILURE
101	15	16	16	51	MODCOMP FAILURE
102	7	56	8	8	MODCOMP FAILURE
103	13	30	13	35	MODCOMP SERVICE
108	6	2	6	3	TOD CORRECTION
115	10	27	10	29	TOD CORRECTION
118	6	2	6	4	TOD CORRECTION
119	9	21	9	27	SYSTEM WORK
119	10	36	11	8	SYSTEM WORK
123	8	45	8	47	TOD CORRECTION
123	6	1	6	3	TOD CORRECTION
124	11	39	11	40	TOD CORRECTION
129	6	0	6	2	TOD CORRECTION
130	6	1	6	2	TOD CORRECTION
132	6	54	7	20	CE. MAINTENANCE
136	6	12	6	13	TOD CORRECTION
142	6	2	6	3	TOD CORRECTION
149	6	5	6	6	TOD CORRECTION
151	6	1	6	2	TOD CORRECTION
159	7	34	7	37	TOD CORRECTION
160	6	1	6	2	TOD CORRECTION
165	10	25	10	26	TOD CORRECTION
166	8	40	8	43	CE MAINTENANCE
168	6	43	7	34	DATA LOST
170	6	1	6	4	TOD CORRECTION
170	13	13	13	14	TOD CORRECTION
173	19	18	21	49	POWER JUMP
174	6	49	6	50	TOD CORRECTION
177	13	20	13	21	SYSTEM WORK
179	6	1	6	2	TOD CORRECTION
179	8	43	8	45	SYSTEM WORK
179	8	46	8	48	SYSTEM WORK
179	8	54	8	56	SYSTEM WORK
179	12	34	12	40	SYSTEM WORK
179	13	7	13	24	SYSTEM WORK
180	6	1	6	2	TOD CORRECTION
185	10	15	10	16	TOD CORRECTION
186	10	52	24	0	MODCOMP FAILURE
187	0	0	24	0	MODCOMP FAILURE
188	0	0	14	51	MODCOMP FAILURE
189	6	22	11	50	MODCOMP POWER FAILURE
189	18	14	24	0	MODCOMP FAILURE
190	0	0	18	31	MODCOMP FAILURE
191	7	13	7	15	MODCOMP FAILURE
191	9	16	9	17	MODCOMP FAILURE
191	10	53	10	54	MODCOMP FAILURE
191	12	43	12	44	MODCOMP FAILURE
191	19	18	19	49	MODCOMP FAILURE
191	20	27	20	29	MODCOMP FAILURE
192	7	6	7	7	MODCOMP FAILURE
192	7	22	8	18	MODCOMP FAILURE
192	10	54	11	58	MODCOMP FAILURE
192	12	56	14	44	MODCOMP FAILURE
193	6	44	9	12	MODCOMP FAILURE
193	10	48	10	49	TOD CORRECTION
193	12	19	12	31	MODCOMP FAILURE
193	13	36	14	20	MODCOMP FAILURE
193	14	43	15	14	MODCOMP FAILURE
193	15	49	15	51	MODCOMP FAILURE
194	6	53	7	24	MODCOMP FAILURE
194	8	11	8	29	MODCOMP FAILURE
194	10	46	10	48	MODCOMP FAILURE
194	11	27	11	41	MODCOMP FAILURE
194	12	12	12	13	MODCOMP FAILURE
194	13	39	14	13	MODCOMP FAILURE

Table II.1.1 Daily DP downtime in the period 1 April - 30 September 1984.

LIST OF BREAKS IN DP PROCESSING THE LAST . HALF-YEAR

DAY	START		STOP		COMMENTS.....
194	14	20	14	23	MODCOMP FAILURE
194	14	26	14	27	MODCOMP FAILURE
194	14	41	14	47	MODCOMP FAILURE
194	15	16	16	26	MODCOMP FAILURE
195	3	18	6	24	MODCOMP FAILURE
195	7	25	7	46	MODCOMP FAILURE
195	10	20	12	46	MODCOMP FAILURE
195	12	54	13	0	MODCOMP FAILURE
196	6	28	6	29	MODCOMP FAILURE
197	10	33	10	34	MODCOMP FAILURE
198	11	7	11	8	TILKOPL. ANALOG
198	12	10	12	30	MODCOMP FAILURE
201	10	40	10	41	MODCOMP FAILURE
202	12	0	12	2	MODCOMP FAILURE
205	6	1	6	3	TOD CORRECTION
207	23	51	24	0	OPER. FAILURE
208	0	0	6	35	OPER. FAILURE
212	6	4	6	6	TOD CORRECTION
216	6	2	6	3	TOD CORRECTION
223	10	47	10	48	TOD CORRECTION
227	6	1	6	10	TOD CORRECTION
230	6	0	6	2	TOD CORRECTION
234	5	39	5	41	TOD CORRECTION
236	8	28	24	0	SYSTEM FAILURE
237	0	0	6	28	SYSTEM FAILURE
241	9	25	9	37	POWER FAILURE
241	15	26	19	49	CE WORK (DISK CH)
242	13	35	13	45	POWER BREAK
243	6	1	6	2	TOD CORRECTION
247	14	17	14	20	SYSTEM FAILURE
250	6	1	6	2	TOD CORRECTION
254	6	1	6	2	TOD CORRECTION
254	9	25	9	30	2701 FAILURE
254	9	40	9	46	2701 FAILURE
255	11	1	11	2	LINE FAILURE
255	11	6	11	7	LINE FAILURE
255	11	22	11	24	LINE FAILURE
255	11	30	11	31	LINE FAILURE
255	19	44	21	28	MODCOMP FAILURE
256	7	52	8	1	MODCOMP TEST
258	3	3	6	5	MODCOMP FAILURE
261	6	0	6	2	TOD CORRECTION
261	6	5	6	6	LINE FAILURE
261	6	40	6	41	LINE FAILURE
261	6	50	6	52	LINE FAILURE
263	6	17	6	19	TOD CORRECTION
263	7	56	10	53	2701 FAILURE
263	12	59	13	0	MODCOMP TEST
264	6	1	6	2	TOD CORRECTION
266	16	20	24	0	2701 FAILURE
267	0	0	13	23	2701 FAILURE
267	13	37	13	39	2701 FAILURE
267	13	50	13	51	2701 FAILURE
268	5	51	7	14	2701 FAILURE
269	6	1	6	2	TOD CORRECTION
270	10	23	10	30	MODEM TEST
270	14	26	24	0	2701 FAILURE
271	0	0	11	43	2701 FAILURE
272	6	1	6	2	TOD CORRECTION
272	6	42	6	48	MODEM TEST
273	14	28	24	0	POWER FAILURE
274	0	0	9	1	POWER FAILURE

Table II.1.1 cont.

Month	DP Uptime (hrs)	DP Uptime (%)	No. of DP breaks	No. of days with breaks	DP MTBF* (days)
Apr	714.08	99.2	16	9	1.8
May	743.48	99.9	10	9	2.8
Jun	715.88	99.4	17	11	1.7
Jul	637.63	85.7	43	20	0.6
Aug	716.98	96.4	10	10	2.7
Sep	649.05	90.1	30	18	0.9
	4177.10	95.1	126	77	1.4

Mean-time-between-failures = (total uptime/no. of up intervals)

Table II.1.2 Online system performance, 1 April - 30 September 1984.

II.2 Array communications

Table II.2.1 reflects the performance of the communications systems throughout the reporting period. Numbers marked with asterisks, indicating high error rates, are commented on in the following paragraphs.

Modcomp stops reported in the previous summary continued in April. Until two communications interface cards were swapped in Modcomp (14 April), 02C and 03C communications systems were suspected as sources of the problems. Frequent tests and interruptions of these communications systems resulted in high error figures during week 15.

On July 10 the MODCOMP processor was moved to another location in connection with preparations for installing new equipment in the computer hall. After reconnection and restart the Modcomp stopped frequently as a result of power supply failure. In addition a bad contact in the plug between the high speed modem and the Modcomp was found.

Although the performance has since improved, we have temporarily lost the ability to automaticallyinitiate resynchronization of the lines after restart. This is not of vital importance, as resynchronization may also be initiated "manually" by the operator using a special option in the online program. The problem will be taken care of when other high priority tasks have been finished (such as modification of the 1950 Interface Handler between the Modcomp and the IBM 4341, etc.).

Summary by month:

Apr — Problem with Modcomp stops continued. 02C, 03C communications systems were suspected. In connection with attempts to solve the problem the systems were frequently affected (tests, etc.), causing discontinuity in their operation. Consequently, high error figures (week 15), 21.4%.

May — Two communication interface cards were swapped in Modcomp (14 Apr) improving the performance drastically. Hence 02C, 03C back to normal operation. 02B was down between week 3 and 4 due to lack of power to the subarray.

June — As a result of power loss (after lightning) 04C was down between 5 and 25 June.

July — In the beginning of July data equipment, including the Modcomp, were moved to other locations in the computer hall, causing Modcomp problems with many stops and high error figures, as indicated in Table II.2.1.

Aug — 04C. Error in data stream last weeks, average 0.13%. NTA Lillestrøm and Hamar checked line. Irregularities were not discovered. Still minor problems with the Modcomp.

Sept — 04C was visited (Oct 3) as communications system still erroneous. Modem replaced without improving the performance. Test indicated line problems.

Also 02B communications system is erroneous. Test result gave us reason to believe the path towards the CTV caused data errors.

02C communications system was down between 11 and 20 September after cable rerouting and movement of equipment caused problems.

Between 15 and 17 September 03C communications system was switched out due to resynch. problems.

06C (NORSAR subarray) will be made operational again as soon as the line and data communications equipoment are checked.

Miscellaneous

Operation of the analog lines from NORESS stations was terminated in the beginning of May. The only analog line in operation is the one from the 02B (Telemetry station) whose performance has been satisfactory.

O.A. Hansen

Sub-array	Apr 84 (4) (2-29.4)	May 84 (5) (30.4-3.6)	Jun 84 (4) (4.6-1.7)	Jul 84 (4) (2-29.7)	Aug 84 (5) (30.7-2.9)	Sep 84 (4) (3-30.9)	Average ½ yr
01A	0.0004	0.0001	0.05	1.796	0.001	0.013	0.31
01B	0.0003	-	0.04	1.597	0.001	0.004	0.274
02B	0.0003	0.028	0.0003	1.972	0.001	6.700	1.45
02C	*5.360	0.0009	0.0006	1.438	0.009	*34.2	*6.835
03C	*4.465	0.0003	0.010	*3.029	0.004	8.03	2.590
04C	0.004	0.0026	*44.8	8.061	0.062	1.50	*9.072
06C	*100.0	*100.0	*100.0	*100.0	*100.0	*100.0	*100.0
AVER	15.69	14.29	20.70	16.84	14.30	21.49	17.22
Less	02C,03C 06C	06C	04C,06C	03C,06C	06C	02C,03C 06C	02C,04C 06C
	0.001	0.005	0.02	2.97	0.013	3.249	1.156

* see item II.2 regarding figures with asterisks

Table II.2.1 Communications performance. Figures in per cent based on total transmitted frames/week (1.2096×10^7). (2 Apr - 30 Sep 1984)

III. ARRAY PERFORMANCE

III.1 Event Processor Operation

In Table III.1 some monthly statistics of the Event Processor operation are given:

	Teleseismic	Core Phases	Sum	Daily
Apr 84	295	58	353	11.8
May 84	321	78	399	12.9
Jun 84	275	52	327	10.9
Jul 84	308	46	354	11.4
Aug 84	331	51	382	12.3
Sep 84	256	89	345	11.5
	1786	374	2160	11.8

Table III.1

Event Processor statistics, Apr - Sep 1984

B.Kr. Hokland

IV. IMPROVEMENTS AND MODIFICATIONS

IV.1 NORSAR on-line system using 4331/4341 and MODCOMP Classic

We refer to the detection processor operation statistics for detailed information about uptime, communications and processing performance.

During this reporting period we had one serious breakdown in the on-line system caused by the MODCOMP. The breakdown occurred after we moved the computer as a result of a reorganization of the computer hall. Service people from the computer company used two days to apparently solve the problem. However, we soon saw a lot of spikes in the data, and a few days later the main problem was located in the power supply. After a new power supply was installed the system has been running very well. A previous problem with 0.5 sec data drop (mentioned in the previous report) also disappeared after the replacement of the power supply.

As a result of bad performance of the old alarm system we have installed a new alarm. The system calls the operator on duty when there is a power break or stop in the communications system. The new alarm system has resulted in a safer reporting of breakdowns in the on-line system and will hopefully result in an improved uptime.

A new telex connection is now available through our SERIES/1 computer. This connection makes it possible for us to create a telex on the computer and then transmit the telex directly into the telex network. As a result of an AFTAC request for more frequent transmission of bulletins, we have implemented an automatic procedure for DPX and EPX transmissions, using the new telex interface. During the past two months our new telex system with

automatic transmission of bulletins has been tested with transmission 3 times a day and 7 days a week. The data are prepared by the event processing system and up-to-date bulletins are transmitted at 0100, 0900 and 1700 GMT.

The NORSAR on-line system is now completely automatic after this telex installation with automatic data collection, real-time data processing, plotting of events and transmission of bulletins.

R. Paulsen

V. MAINTENANCE ACTIVITIES

V.1 Activities in the field and at the Maintenance Center

In the period P.W. Larsen has devoted much time to tasks related to NORESS. He has participated in meetings with consultants and contractors, field surveys and field installations. Also administration and support in connection with the U.S. team from Sandia and Comsat, etc., has taken part of his time.

Visits to the subarrays have been limited to cases of more or less "acute" character, affecting the operation of a whole subarray, such as power loss, failing modems, or other situations and incidents which needed NMC assistance. On the other hand, personnel at the computer center have been able to adjust most LP seismometers which were out of adjustment. By means of data collection and analysis programs reduced performance and malfunctions could be discovered.

Table V.1 indicates the visits made to subarrays in the period.

Subarray/ area	Task	Date
02B (Telemetry)	St 01, ch 23. Bad performance mainly caused by a bad discr/receiver NDPC	12 Apr
02B	Visited in connection with power failure	4 May
04C	-"-	Jun
01A	SP04 cable rerouted and spliced	20 Aug

Table V.1 Activities in the field and at the NORSAR Maintenance Center (Apr - Sep 1984).

V.2 Improvements and modifications

No changes have been made in the NORSAR or NORESS arrays.

Recording of analog data from the provisional NORESS array was terminated at the beginning of May 1984.

V.3 Array status

As of 30 September 1984 the following channels deviated from tolerance:

01B	05, 08, 06C (not in operation)	
03C	08	
04C	09	
01A	01	8 Hz filter
	02	-"-
	04	AH. 30 dB

O.A. Hansen

VI. DOCUMENTATION DEVELOPED

Doornbos, D.J.: Solutions and station residuals from long-period waveform inversion of deep events. Submitted for publication.

Husebye, E.S., S.F. Ingate & E. Thoresen: Seismic arrays for everyone. Submitted for publication.

Husebye, E.S. and S.F. Ingate: Seismic arrays - a new rennaissance. Submitted for publication.

Ingate, S.F., E.S. Husebye and A. Christoffersson: Regional arrays and optimum processing schemes. Submitted for publication.

Tronrud, L.B.: Semiannual Tech. Summary, 1 Oct 1983 - 31 Mar 1984, NTNF/NORSAR, Kjeller, Norway.

L.B. Loughran

VII. SUMMARY OF TECHNICAL REPORTS/PAPERS PREPARED

VII.1 Source solutions from long-period waveform inversion

Seismic waveform inversion techniques are being applied to determine source parameters, and to determine the parameters describing earth structure. This requires (1) a suitable source parameterization, and (2) a suitable device to account for earth structure effects in waveform modelling. Moment tensor techniques offer a partial solution to the first problem since the source type need not be specified a priori, whereas model-dependent constraints can still be used in the inversion. A remaining problem is that a moment tensor method in practice involves a point source inversion technique, i.e., solutions are obtained with a reference to a point $(\underline{\xi}_o, \tau_o)$. In previous work aimed at the determination of source finiteness, a particular partorization of the moment tensor stress glut was used:

$$\dot{m}_{jk}(\underline{\xi}, \tau) = M_{jk}\, f(\underline{\xi}, \tau) \qquad (1)$$

and the source finiteness is contained in $f(\underline{\xi}, \tau)$. However, the effect of source finiteness can usually be neglected in long-period waves from sources of up to moderate size. Alternatively, if the effect is known (or assumed), it can be directly included in the Green's functions. In these circumstances, a useful approximation to the far-field response is a sum of terms of the form

$$u_i(\underline{x}, t) = M_{jk}\, G_{j,k}^{\,i}(\underline{\xi}_o, \underline{x}, t-\tau_o-\delta\tau_i) \qquad (2)$$

where $G_{j,k}^{\,i}$ is a modified Green's function, and the time delay $\delta\tau_i$ depends on the mislocation of the source. In practice, the use of an imperfect earth model in computing $G_{j,k}^{\,i}$ also leads to a time residual, so we can write

$$\delta\tau_i = \underline{\zeta_i}^T \underline{F}_{(1)} + d_i \qquad (3)$$

where $\underline{F}_{(1)}$ is the mislocation vector, $\underline{\zeta_i}$ is a slowness vector, and d_i is often called a station residual.

The straightforward approach to solve for $\delta\tau_i$ in equation (2) is by a correlation method, e.g., Ward (1983). In the iterative method we use, M_{jk} is estimated by a least squares inversion of the normalized records; this estimate is used in forming synthetics which are correlated with the observed waveforms to determine $\delta\tau_i$, etc. With shallow sources, where the observed records are modelled by a superposition of direct and depth phases, the correlation method should be applied for a range of depths.

Fig. VII.1.1 illustrates the applicaiton of this method to a deep event in the Fiji Islands region. Rather than showing the complete moment tensor, the equal area projection to the right shows only a double couple approximation. However, results on deviations from the double couple for 12 events are summarized in Fig. VII.1.2. Figs. VII.1.2a, b and c were obtained by slightly different inversion procedures, and the result in somewhat different deviations. Our presumably best solutions are in Fig. VII.1.2c, and we conclude that at this stage there is no compelling evidence for significant deviations from the double couple mechanism of these deep earthquakes (c.f. Giardini, 1984).

The method also leads to an estimate of the centroid time shift $\Delta\tau_o$ which is one of the components of the mislocation vector, and which is related to source finiteness. The centroid time shifts are shown in Fig. VII.1.3 together with the time difference between the short-period P onset and the long-period P correlation lag. The theoretical relation would be of the form

$$\delta\tau_o - b(M/\Delta\sigma)_{1/3} \qquad (4)$$

and for a circular fault with directivity coefficient d = 1.5 (Doornbos, 1984) and relevant P and S velocities: $b = 17.2\times10_{-9}$ where M is in dyne.cm and $\Delta\tau$ in bar. Comparison with the results in Fig. VII.1.3 then suggests that the data are consistent with a stress drop in the range 10-100 bar.

D.J. Doornbos

References

Doornbos, D.J. (1984). On the determination of radiated seismic energy and related source parameters, Bull. Seism. Soc. Am., 74, 395-415.

Giardini, D. (1984). Systematic analysis of deep seismicity: 200 centroid-moment tensor solutions for earthquakes between 1977 and 1980, Geophys. J.R. Astr. Soc., in press.

Ward, S.N. (1983). Body wave inversion: Moment tensors and depths of oceanic intraplate bending earthquakes, J. Geophys. Res., 88, 9315-9330.

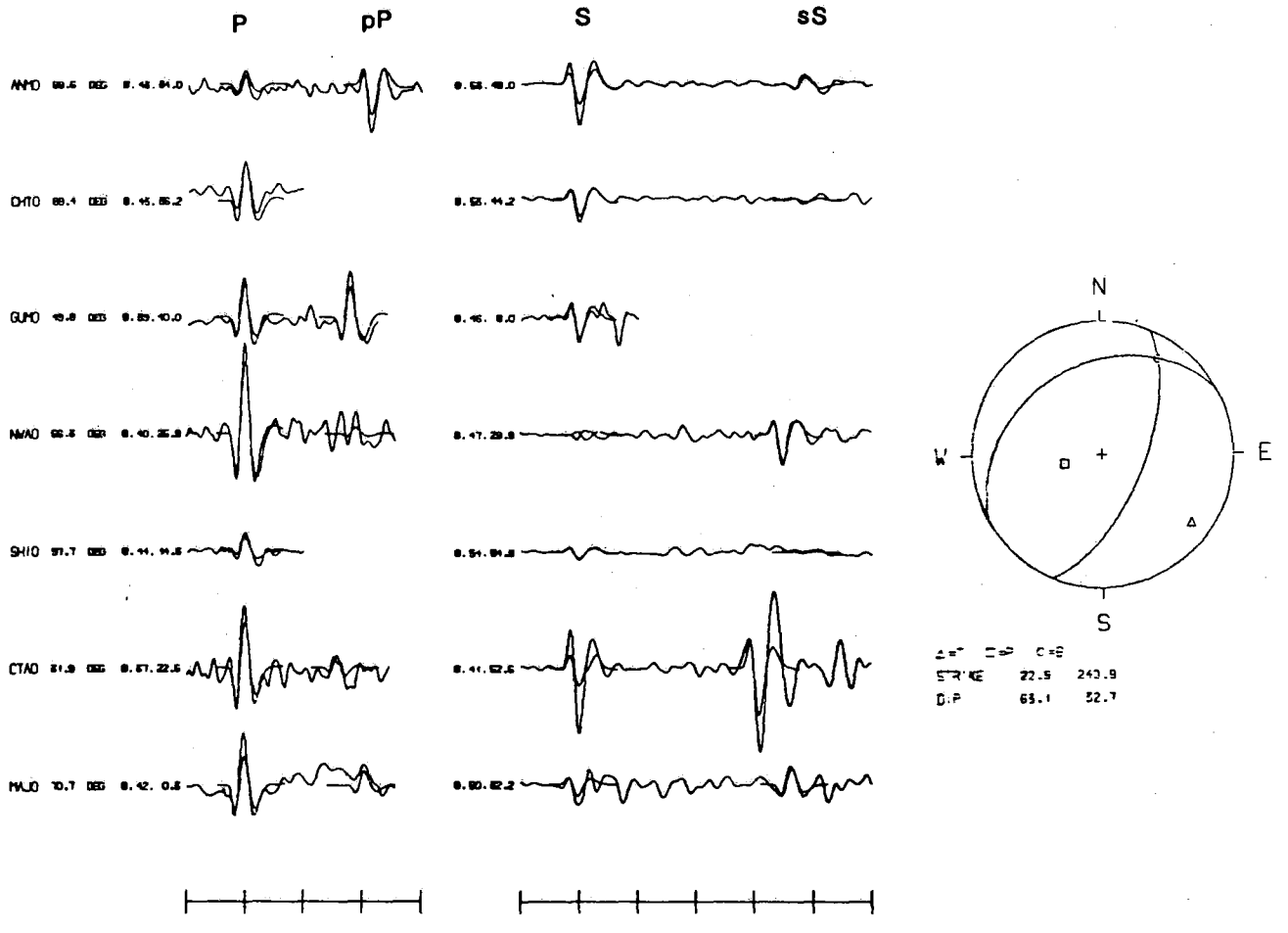

Fig. VII.1.1 Vertical and transverse component records from stations of the GDSN network, showing P, pP, SH and sSH from a deep m_b 5.6 event in the Fiji Islands region. Synthetic record sections for the moment tensor point source solution are plotted over the observed records. To the right, the equal area projection of a double couple approximation to the moment tensor.

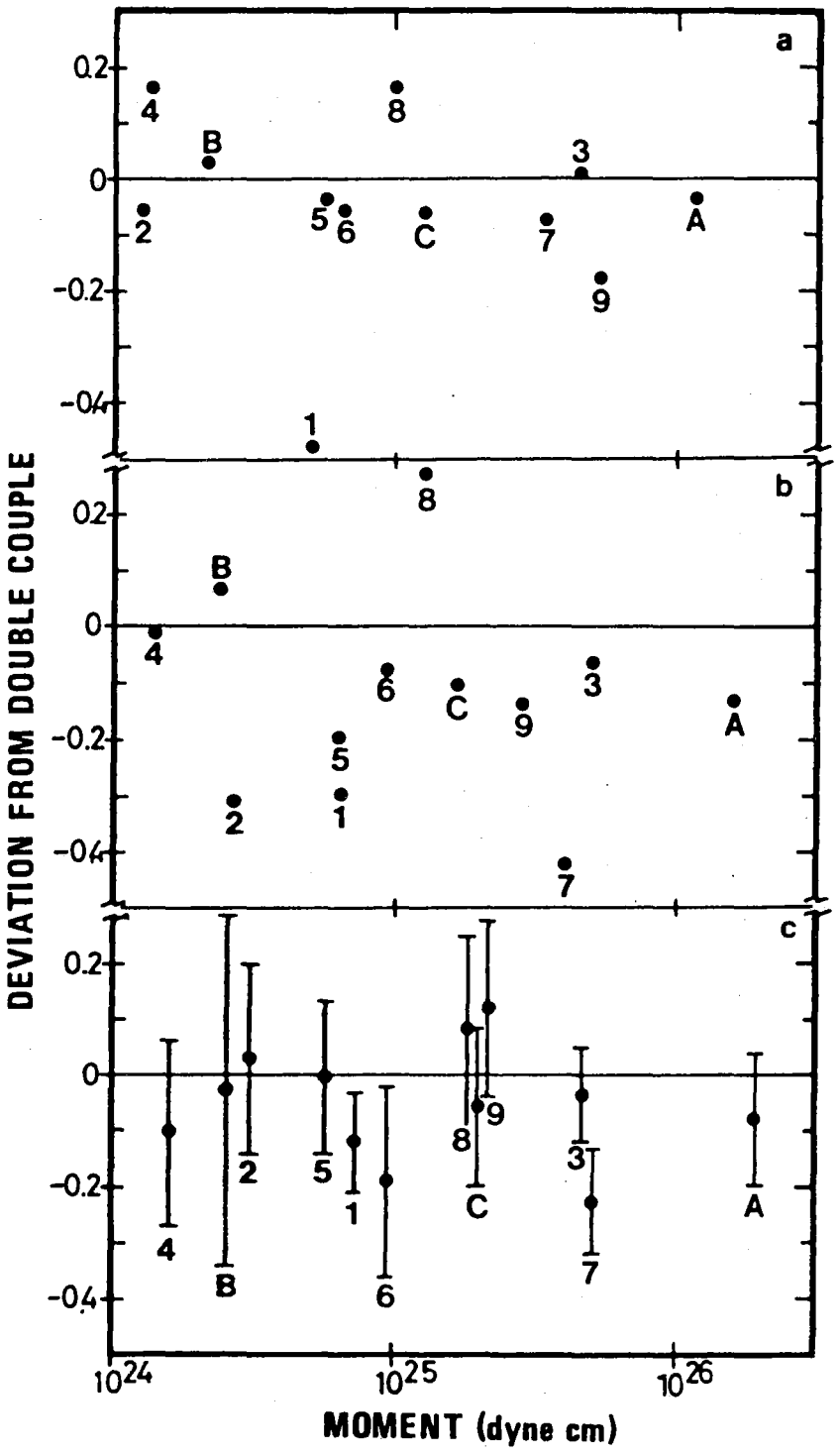

Fig. VII.1.2 Deviation from the double couple versus the seismic moment for 12 deep events in the Fiji Islands region. The deviation is given by λ_3 / λ_1 where $|\lambda_1|$ and $|\lambda_3|$ are the largest and smallest absolute eigenvalue of the moment tensor. A positive/negative deviation corresponds with λ_1 being the compressional/tensional eigenvalue. The results in a, b and c represent different moment tensor inversions but the best solutions, with standard deviations, are given in c.

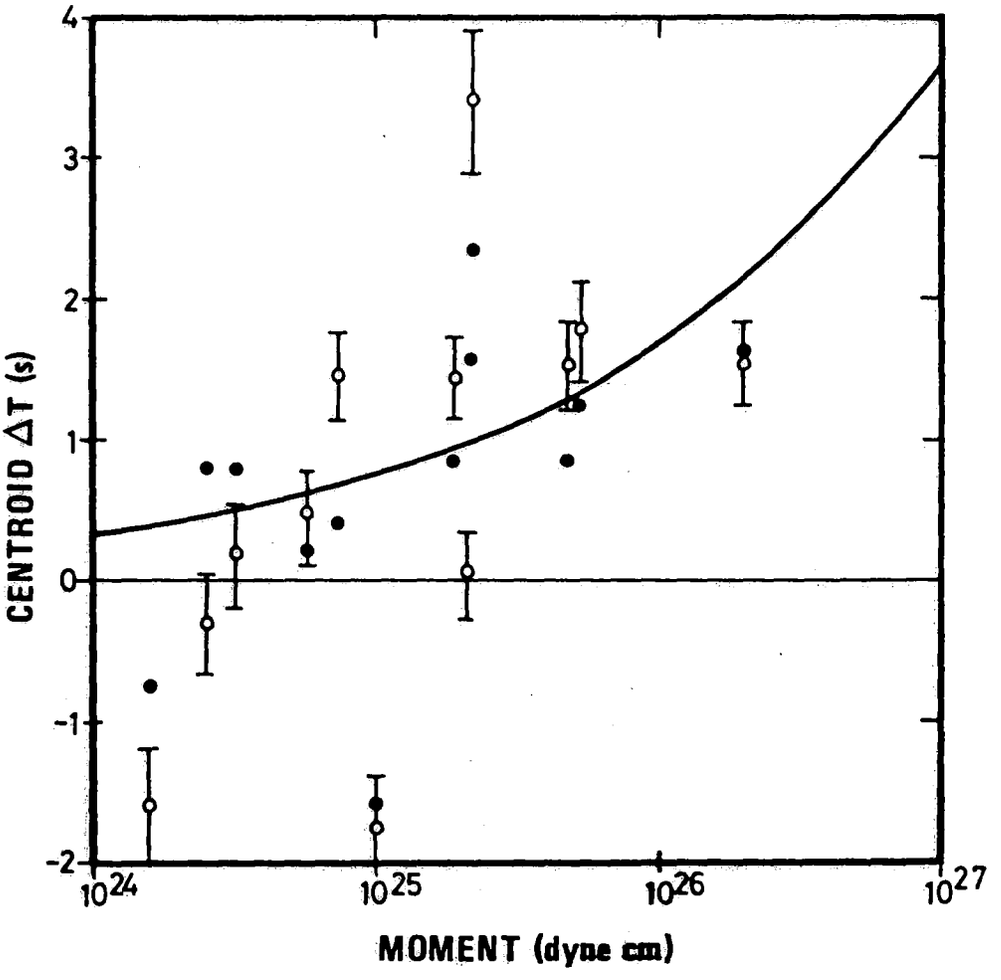

Fig. VII.1.3 O: Centroid time shift versus moment of the deep events referred to in Fig. VII.1.2. ●: Averaged difference between short-period P onset and long-period P correlation lag. The solid line is a theoretical relation of the form $\Delta\tau_o = c\ M_o^{1/3}$, with $c = 3.6\times10^{-9}$ s/(dyne.cm)$^{1/3}$.

VII.2 Some path effects and long-period station residuals in the GDSN network

In present-day routine methods of source analysis (Dziewonski and Woodhouse, 1983), intrinsic source parameters and the mislocation of the source can be determined simultaneously from long-period records, for a fixed earth model. It has been argued that lateral relocation of events is often needed not so much for the purpose of correcting real mislocations, but rather as a device to compensate for the travel time or phase delay effects of anomalous earth structure. The implication of this argument is in accordance with other findings indicating that, away from critical zones, the main effect of velocity anomalies is often on the travel times of ray contributions to the long-period body waves (e.g., Wallace, 1983). A logical consequence of this line of reasoning is to try and simultaneously determine intrinsic source parameters and travel time residuals rather than source location. The formulation of this procedure is outlined in a comparison contribution (see also Doornbos, 1984). We analyze the travel time residuals $\delta\tau_{ij}$ by writing them in the form

$$\delta\tau_{ij} = \underline{\zeta}_{ij}^{T}\, \underline{F}(1)_{ij} + d_i \qquad (1)$$

where $\underline{F}(1)$ is the mislocation vector of the source, $\underline{\zeta}$ is a slowness vector, and i and j denote the source and receiver, respectively. Our present analysis of station residuals uses PREM as the reference model. Since we keep the velocity model fixed, all propagation path effects are lumped into the station term d_i. The station term is different for P and S waves, but for the moment we will assume that it is otherwise constant.

We can eliminate the depth mislocation term in equation (1). Furthermore, in the present work we have kept the lateral location of the source fixed. The only remaining term is then the centroid time shift $\Delta\tau_{o,j} - (\tau_o - \tau_o)_j$. There is a natural nonuniqueness of the division of time delay in terms in equation (1). In terms of our simplified relation, it means that the only constraint on the average of station residuals d is that

$$\overline{\delta\tau} = \overline{\Delta\tau_o} + \overline{d}$$

Using a data set from 12 deep events in the Fiji Islands region, we have measured the time difference between the short-period P onset and the long-period correlation lag. The average of these differences for each event is taken to be a measure of $\Delta\tau_{o,j}$; the average over all events is then a measure of $\Delta\tau_o$. The system of equations (1) has been solved with this constraint for $\Delta\tau_o$, and the resulting station residuals for P and S waves are given as a function of epicentral distance in Fig. VII.2.1. Typical observational features are the base line effect for P and S, the trend with epicentral distance, especially for S, and the travel time anomalies for S at some of the stations. All of these features need further investigation, but modifications to the reference model (including the absorption band used) seem inevitable.

We note that not only the time residuals, but also the amplitude residuals are significant. The amplitude residue is defined as the amplitude ratio observed/predicted where the prediction is based on the moment tensor solution and the residence is an average over the events, i.e., it is the least squares estimate based on the individual residuals as obtained from each moment tensor solution. Fig. VII.2.2 shows the amplitude residues of P and Fig. VII.2.3 those of SH, but we have plotted the residues for direct (P and SH) and depth phases (pP and sSH) separately. There is no clear correlation with distance, but there is a clear difference between the residuals for direct and depth phases, especially for SH. In light of these results, we would have to consider necessary modifications of in particular the upper mantle in the source region.

D.J.Doornbos

References

Doornbos, D.J. (1984): Source solutions and station residuals from long-period waveform inversion of deep events. Submitted for publication.

Dziewonski, A.M. and J.H. Woodhouse (1983): An experiment in systematic study of global seismicity: Centroid-moment tensor solutions for 20 moderate and large earthquakes of 1981. J. Geophys. Res., 88, 3247-3271.

Wallace, T.C. (1983): Long-period regional body waves, Ph.D. Thesis, Cal. Inst. Tech.

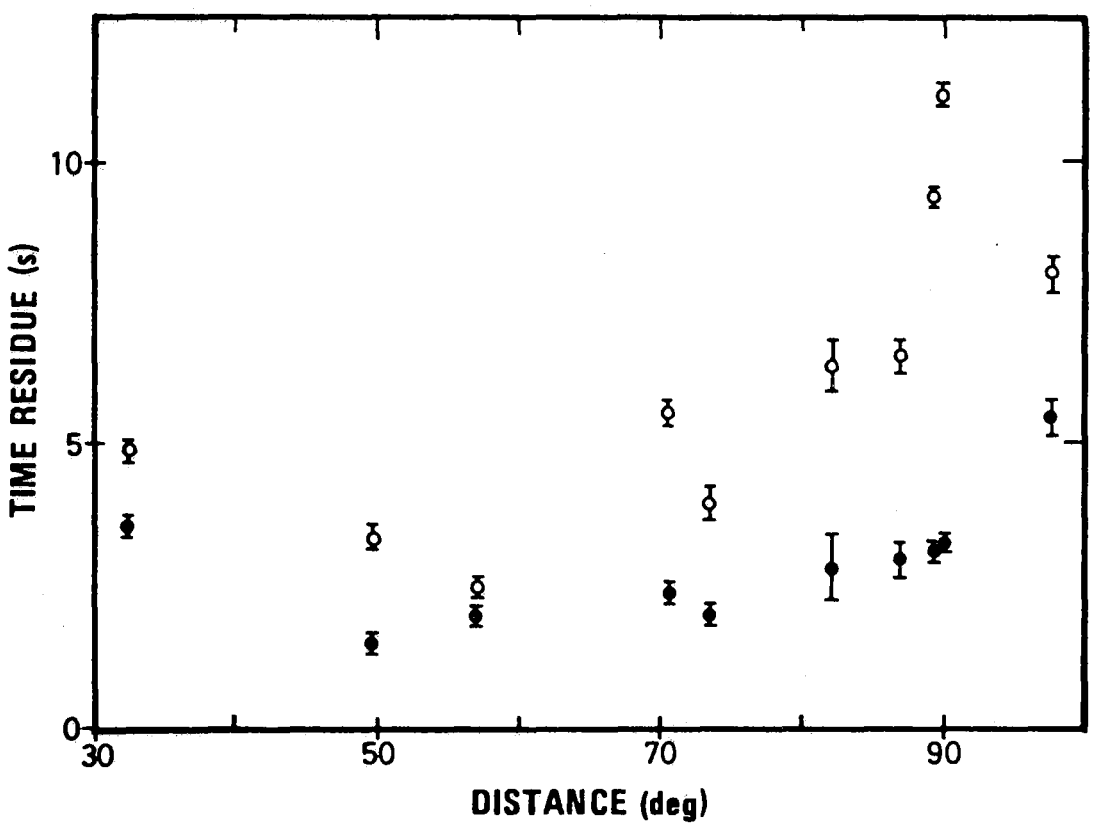

Fig. VII.2.1 Travel time residues for long-period P (●) and SH (o) at stations in the GDSN network. The residues apply to deep events in the Fiji Islands region. They are defined as the time difference observed-predicted, and the average of direct and depth phases is taken. Stations are positioned at their average distance from the events.

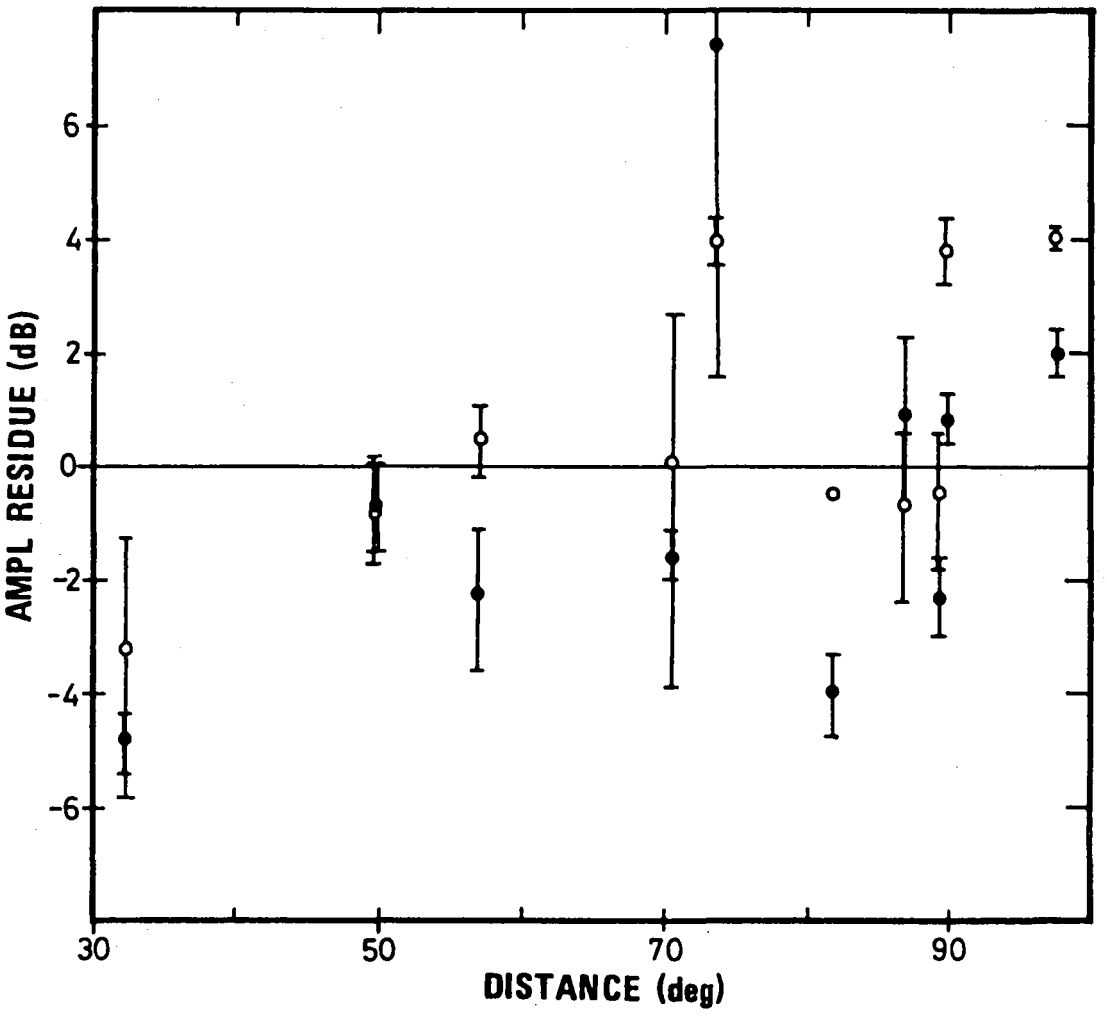

Fig. VII.2.2 Amplitude residues for long-period P (•) and pP (o) at the GDSN stations as in Fig. VII.2.1. The residue is defined as the amplitude ratio observed/ predicted. Stations are positioned at their average distance from the events.

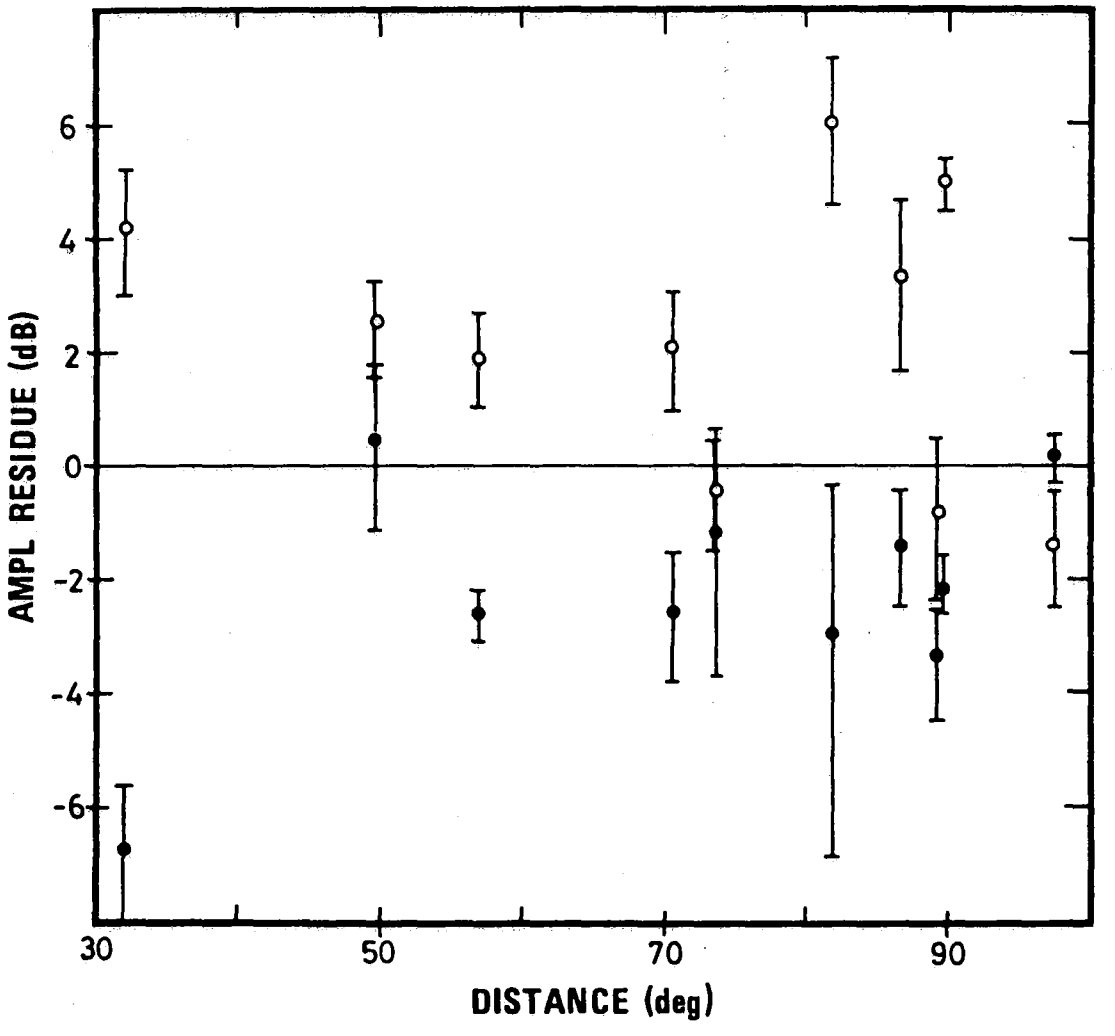

Fig. VII.2.3 Amplitude residues for long-period SH (•) and sSH (o) at the GDSN stations as in Fig. VII.2.1. Other details as in Fig. VII.2.2.

VII.3 Preliminary report on a method of dynamic ray tracing

The project, started in October 1983, is still in progress. The objective is numerical implementation of the methods of dynamic ray tracing (of seismic waves) developed by the author. These methods encompass (1) propagation through caustic regions; (2) edge diffraction; (3) the effects of anisotropy and prestress.

Algorithms and FORTRAN programs for kinematic ray tracing and dynamic ray tracing have been worked out by A. Hanyga. Preliminary testing against simple analytical models (SATM2, SATM3) has been carried out by A. Hanyga on IBM at NORSAR, partly in collaboration with O.A. Sandvin. Testing against realistic models has been done by Dr. Jan Pajchel at the Seismological Observatory, University of Bergen, on VAX.

The programs trace rays and signals in arbitrary user-supplied models. The models are represented by model data files and by a library of subprograms called by the ray tracing programs. We now describe various aspects of the methods applied.

Dynamic ray tracing through caustic regions

It has been shown by Hanyga (1984, 1984a, 1984b, 1984c) that dynamic ray tracing can be generalized to cover the case of WKBJ signals propagating through caustic regions. The generalized DRT consists of integrating a system of ordinary differential equations and is based on a natural extension of the WKBJ method originated by Maslov (Maslov 1972) in quantum mechanics (see Chapman & Drummond, 1982, for an alternative application of the Maslov-WKBJ method in the theory of seismic wave propagation).

The wavefield at a receiver situated at some distance from the caustics is evaluated by tracing the signals along the rays connecting the receiver to the source. The field at a point close to a caustic is given by a diffraction integral whose integrand can be evaluated by tracing along a family of rays.

At a distance from the caustics DRT is carried out by integrating the usual system of ordinary differential equations along a ray. The unknown functions include the parametric equation of the ray (in terms of the travel time parameter), slowness, wavefront curvature matrix and geometric ray spreading referred to the ray-centered coordinates as defined by Hanyga (1982). In the case of S waves the polarization angle is also included. This task is performed by a special subprogram of the DRT program.

Whenever the absolute value of the geometric ray spreading J turns out to be smaller than a positive number ε a canonical transformation in the phase space of position and slowness vectors is performed and a transformed version of the DRT equations is integrated. This task is performed by another DRT subprogram. As soon as the geometric ray spreading exceeds $\varepsilon > 0$ the original DRT is resumed.

The transformation of the phase of the signal implicitly contains the phase shifts at the caustics. This is a nontrivial advantage of the method in the case of anisotropic media where the phase shift cannot be guessed by a simple argument (see Chapman & Drummond, 1982, in the case of isotropy).

The transformations referred to above are purely algebraic. The DRT system for the caustic regions differs from the usual one merely by the number of equations (12 instead of 10). In the case of a ray which does not exactly touch a caustic the transformation improves the accuracy.

Boundary conditions are taken from Hanyga (1984a) and initial conditions (at point sources) from Hanyga (1984d). DRT programs have been designed, but testing has not been completed yet.

Edge diffraction

The DRT programs described above allow dynamic ray tracing of edge-diffracted rays from the source to a receiver lying in the shadow of WKBJ rays of a specified kind. An edge-diffracted ray is traced by the method described in the previous section from the edge point to the receiver. At the edge an appropriate version of Snell's law is satisfied and the amplitude is multiplied by the appropriate diffraction coefficient (Hanyga, 1985).

For signal paths in the transition zone of a shadow boundary uniform asymptotic formulae involving Fresnel integrals are used (Achenbach et al, 1982; Hanyga, 1985).

Anisotropy and prestress

The references quoted in the two previous sections deal with arbitrary anisotropic and possibly prestressed linear elastic media. FORTRAN programs based on these references cover the cases of isotropic blocks, transversely isotropic blocks with fixed orientation and with variable orientation of isotropy axes. Detailed formulae for transversely isotropic media are taken from Hanyga, unpublished.

Kinematic ray tracing in 3D

Preliminary to DRT a ray with a prescribed ray code is traced from the point source to the receiver. The associated two-point boundary value problems are solved in the following steps.

Step 1. A large collection of piecewise straight rays is traced through a number of more important interfaces. These include all the efficient reflectors in the model. At each of these interfaces the ray splits into transmitted, equal-angle reflected and two converted reflected rays (the latter are not traced by some programs). The rays are intercepted at their intersection with a surface, a sphere or a cylinder and stored on files.

Step 2. The rays from the above files are used as approximate rays in iterative programs tracing rays through homogeneous isotropic blocks. Polak's algorithm (Polak, 1974) is used. Edge-diffracted rays are traced by the same program.

Step 3. The result of the iterative procedure of Step 2 is fed into a program tracing rays through inhomogeneous and possibly anisotropic blocks. The algorithm is based on the idea of parallel shooting and tracing in fictitious time (Hanyga, 1984a) and uses Polak's version of the method of secants (Polak cit.).

The iterative program through isotropic homogeneous blocks takes 20-30 seconds in the SATM2 models. The programs of Step 3 take a few minutes to run.

A. Hanyga, NTNF Postdoctorate Fellow
(On leave of absence from Institute of Geophyscis, Warsaw, Poland)

References

Achenbach, J.D., A.K. Gautesen & H. McMaken (1982): Ray Methods for Elastic Waves in Solids, Pitman, London.

Chapman, C.H. & R. Drummond (1982): Body wave seismograms in inhomogeneous media using Maslov asymptotic theory, Bull. Seism. Soc. Am., 72, 8277-8317.

Hanyga, A. (1982): Dynamic ray tracing in anisotropic media, Tectonophysics, 90, 243-251.

Hanyga, A. (1984): Dynamic ray tracing in the presence of caustics, I-II, Acta Geophysica Polonica 32.

Hanyga, A. (1984a): Transport equations for an anisotropic elastic medium in the presence of caustics, Gerlands Beitr. Geophysik (Leipzig) 93, 2186-2216.

Hanyga, A. (1984b): Dynamic ray tracing on Lagrangian manifolds, Geophys. J.R. astr. Soc. 79.

Hanyga, A. (1984c): Numerical computation of elastic wavefields in anisotropic elastic media in the presence of caustics, in "Hybrid Methods in Elastic Wave Propogation and Scattering", Proc. NATO Workshop in Castel Gandolfo Aug-Sept 1983, L.B. Felsen (ed.), Martinus Nijhoff, The Hague.

Hanyga, A. (1984d): The point source in an anisotropic elastic medium, Gerlands Beitr. Geophysik 93.

Hanyga, A. (1985): Dynamic ray tracing of edge-diffracted waves, Gerlands Beitr. Geophysik (submitted).

Keller, J.B. (1958): Geometric theory of diffraction in "Calculus of Variation and its Applications", Proc. Symp. in Applied Mathematics, Vol. 8, L.M. Graves (ed.), AMS, Providence, R.I.

Maslov, V.P. (1972): Théorie des perturbations et méthodes asymptotiques, Dunod and Gauthier-Villars, Paris.

Polak, E. (1974): A globally converging secant method with applications to boundary value problems, SIAM J. Numer. Analysis, 11, 529-537.

VII.4 Regional arrays and optimum data processing schemes

In a series of contributions (see reference list) we have addressed various aspects of array design, data processing schemes and past, present and likely future developments in this field. The research to be reported here is tied to an evaluation of the prototype regional array NORESS (configuration shown in Fig. VII.4.1). In this respect a two-fold analyzing strategy was chosen, namely, first to estimate from NORESS data standard noise and signal characteristics like correlation functions and spectra under a variety of conditions/events and secondly, with a basis in Wiener filtering theory, to evaluate the relative merits of various array data processing schemes for SNR-enchancements. In the following the essence of results obtained will be presented.

Noise and signal characteristics

SNR-spectra for events in different tectonic environments are presented in Fig. VII.4.2a,b,c; evidently only P-waves with a predominant shield path exhibit a significant amount of high-frequency energy so as to produce peaks in the SNR-spectra above 5 Hz. Signal paths in oceanic and mobile tectonic belt types of lithosphere appear to be depleted in high-frequency signal energy; the spectra here are not too different from those typical of teleseismic events.

Noise spectra between 2-10 Hz appear to decay like ω^{-4}, and besides that are generally independent of time of day, day of week and seasonal variations as well. In other words, the high-frequency part of the noise field is not dominated by cultural and microseismic noise contributions.

Noise correlations as functions of sensor separations have to be calculated under a variety of conditions, that is, sensor time lags tied to both vertical and horizontal beams. Despite large fluctuations in individual estimates here, significant differences exist as a function of beam location, e.g., see Figs. VII.4.3a and b. This feature is rather obvious from Table

VII.4.1, where SNR-enhancements as a function of phase velocity and azimuth for different bandpass filters and processing schemes amounts to approximately 3 dB!

Array data processing schemes

Within the general class of Wiener filtering 3 array data processing schemes have been considered, namely, standard beamforming, optimum weighting and maximum likelihood (ML) filtering. The mathematics of these approaches are detailed in Ingate et al (1985). Standard beamforming is optimum for uncorrelated noise ($\sqrt{N}$ gain) which in general takes place above 4 Hz for the NORESS array configuration. Optimum weighting may give an additional 2-4 dB gain for correlated noise, while ML-processing is clearly superior vis-à-vis the other two processing schemes, as evident from Fig. VII.4.4. The well-known problem with more advanced array data processing schemes is their rather severe computer loads. For example, for the optimum weighting scheme the noise covariance matrix has to be updated each 2.5-5.0 sec because of a general noise non-stationarity as illustrated in Fig. VII.4.5.

Discussion

After extensive analysis and processing of the NORESS data, some remarks on regional array design and operation may be justified. First of all, array design is problematic as the operational bandwidth reflecting SNR-spectra from different tectonic regimes should cover roughly the 3-8 Hz range in contrast to "teleseismic" arrays, where the bandwidth is 1-2 Hz. To ensure adequate seismicity surveillance capabilities in the 3-8 Hz band very many beams have to be formed, otherwise signal decorrelation losses would be severe, even when the data processing is restricted to simple beamforming. Indeed, if relatively better performance is desired, this may most easily be achieved on the hardware side by adding more instruments and/or using the "analog sensor clustering" commonly used in seismic land surveys. As regards array configuraiton per se, a reasonably flat sensor spacing distribution has to be ensured if we want a reasonably

flat array response as a function of frequency. For example, from Fig. VII.4.4 we see that the NORESS performance is far from optimum below 4 Hz due to high noise correlation and likewise beyond 6-8 Hz due to poor signal correlations.

Arrays are relatively costly to build and operate so there have been limited possibilities for practical experimentation. However, taking advantage of recent advances in microprocessor and communication technology, it is feasible to construct and deploy small, inexpensive arrays as discussed in detail by Husebye et al. This would naturally add to the flexibility of practical array experiments, and also increase the number of arrays being operative. Apparently, most of the seismological community takes part in these new developments as the newly formed IRIS-consortium plans for a digital, global seismograph network and mobile seismic arrays comprising hundreds (thousands) of instruments. These and likely future trends in digital seismometry are discussed in all papers referenced below.

Result summary of the prototype NORESS evaluation

The major problem here was that of suppressing ambient noise, and major results obtained are as follows.

Signal and noise field characteristics

- SNR spectra peak at ca 2, 3 and 6 Hz, respectively, for events whose signal paths are predominantly oceanic, mobile cratonic belt and shield. Teleseismic arrays like LASA and NORSR operate generally in the narrow 1-2 Hz band.
- Above 2 Hz noise spectra are essentially time invariant and besides have approximately a ω^{-4} decay rate in the 2-10 Hz band.

- Noise correlation distance is clearly frequency dependent and is such that noise suppression by simple beamforming will be degraded relative to $\sqrt{N}$ up to about 4 Hz.
- The noise field cannot be considered stationary even for short windows of 2.5-5.0 sec. This is most easily seen in standard beamforming gain variation up to 3 dB as a function of beam location or azimuth and phase velocity.
- Signal correlations for P and Lg phases decrease with increasing sensor separation becoming ca 0.5 at about 3 km. This in combination with steering delay errors, including insufficient number of beams deployed, would severely affect array performance above 6-8 Hz.
- Horizontal seismometer recordings exhibit noise and signal correlations, etc., roughly similar to that observed for vertical instruments.

Noise suppression schemes - variants of Wiener filter theory

- Simple beamforming is optimal or $\sqrt{N}$ for uncorrelated noise, but this cannot be achieved using all instruments due to the relatively small NORESS array aperture of 3 km.
- Optimum weighting based on characteristics as manifested in the noise covariance matrix (multichannel) will give an additional gain of 2-4 dB relative to standard beamforming up to about 5 Hz. A simplification here, reducing these weights to the 0/1-type, gives 1-2 dB less gains but still better than standard beamforming.
- Maximum likelihood filtering, computationally demanding, gave approximately $\sqrt{N}$ gains even for lower frequencies where simple beamforming was inefficient.

On the basis of the above results and technical considerations as well, our conclusion is that seismic surveillance is most effectively attained by deploying rather many seismometers (regional arrays) combined with simple processing schemes rather than few

instruments combined with sophisticated processing schemes like ML-filtering - simply because investments in array hardware are considered more cost-effective than array software investments.

E.S. Husebye
S.F. Ingate (NTNF Post-doctorate Fellow)
A. Christoffersson
(Uppsala University)

References

Husebye, E.S. and E. Thoresen (1984): Personal seismometry now! EOS, 65, 441-442.

Husebye, E.S., E. Thoresen and S.F. Ingate (1984): Seismic arrays for everyone. Terra Cognita (in press).

Husebye, E.S. and S.F. Ingate (1984): Seismic arrays - a new renaissance (in press).

Ingate, S.F., E.S. Husebye and A. Christoffersson (1984): Regional arrays and optimum data processing schemes. Submitted for publication.

Filter (Hz)	Phase velocity (km s^{-1})	Azimuth (deg)	Gain (dB) Std. beam	0-weighting
1.0-3.0	4.60	0	3.63	4.82
		90	2.46	3.56
		180	3.94	5.41
		270	5.24	7.15
1.5-3.5	6.20	0	6.50	7.50
		90	5.34	6.61
		180	5.25	6.04
		270	6.71	7.88
2.0-4.0	8.10	0	10.0	11.37
		90	8.82	10.23
		180	7.81	8.94
		270	9.79	10.97
2.5-4.5	12.0	0	11.29	13.90
		90	10.42	12.38
		180	9.94	11.94
		270	11.14	13.36

Table VII.4.1 Standard beamforming and optimum weighting gains as functions of primarily azimuth but also phase velocity and filter passband. The thirteen NORESS-sensors used were nos. 1, 5 to 9 and 10 to 16. Azimuthal gain variation amount to approximately 2 dB, which may increase 1 dB if finer azimuth sampling intervals of 30 deg had been used.

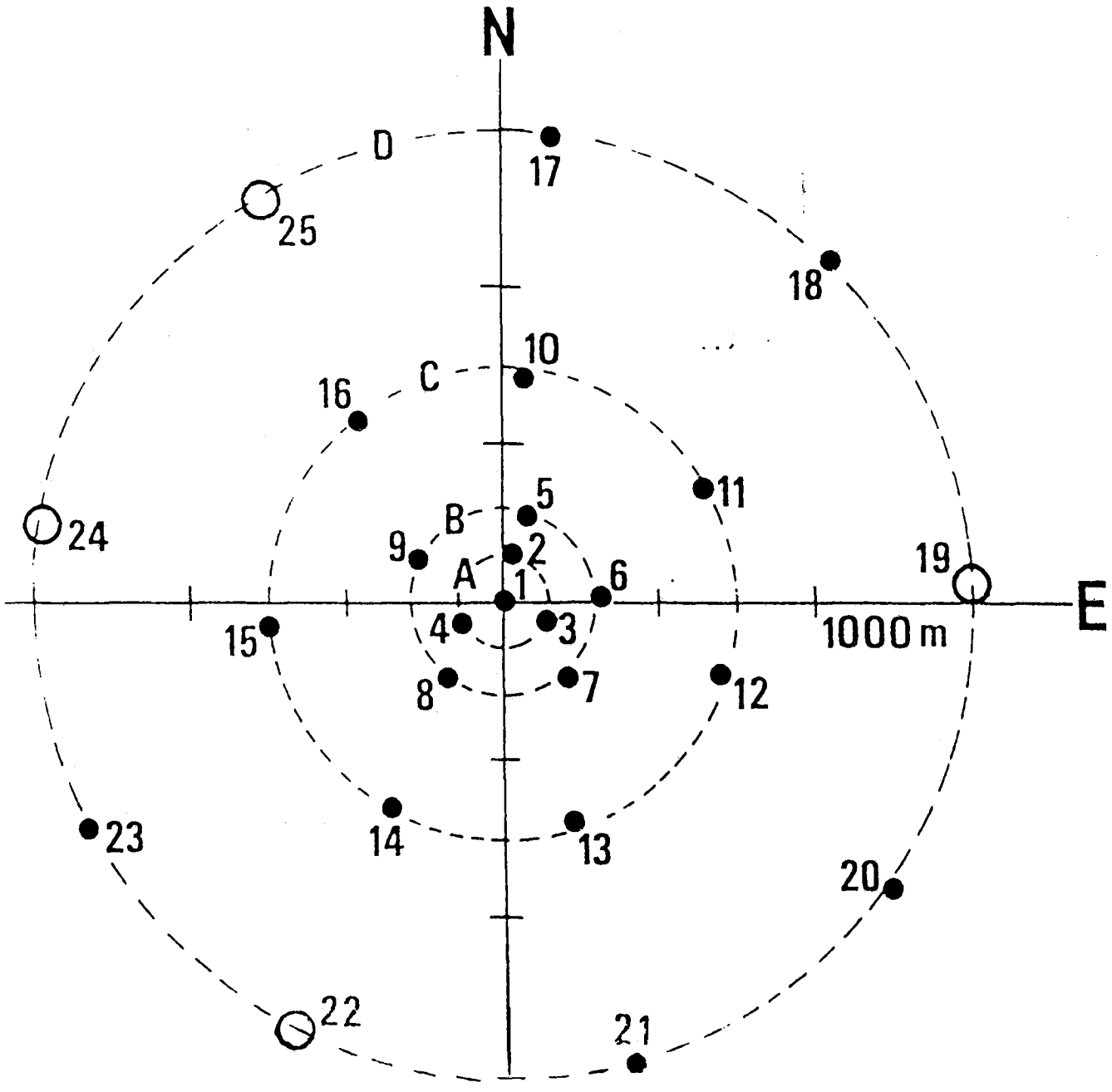

Fig. VII.4.1 The experimental NORESS array located near NORSAR site 06C. Instruments at sites indicated by open circles will be in operation in late 1984.

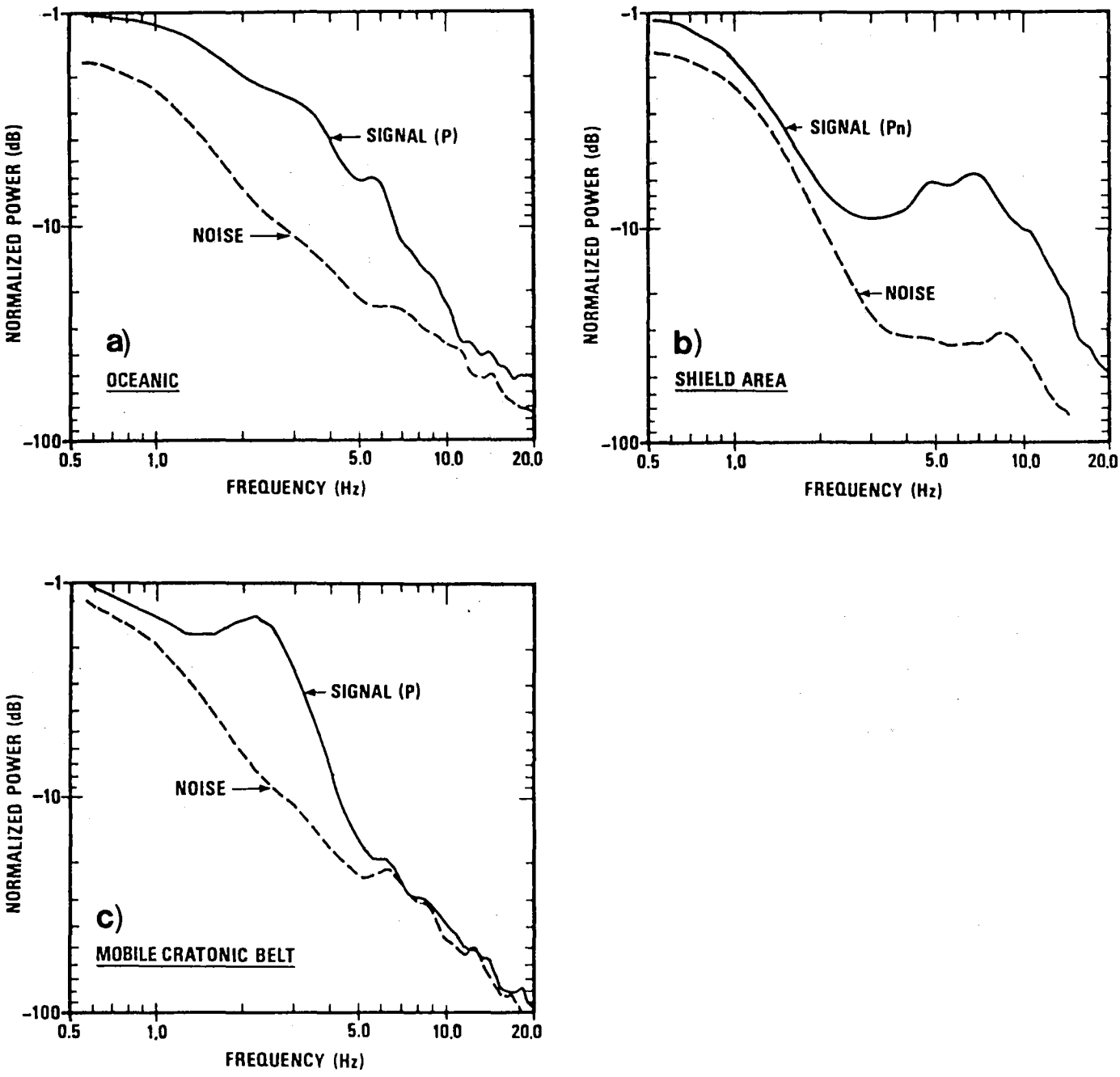

Fig. VII.4.2 Power spectra of events recorded by NORESS. Also shown are spectra of noise before event arrival. Each represents a spectrum averaged over 21 sensors. a) oceanic events; b) shield events; c) events within mobile cratonic belts.

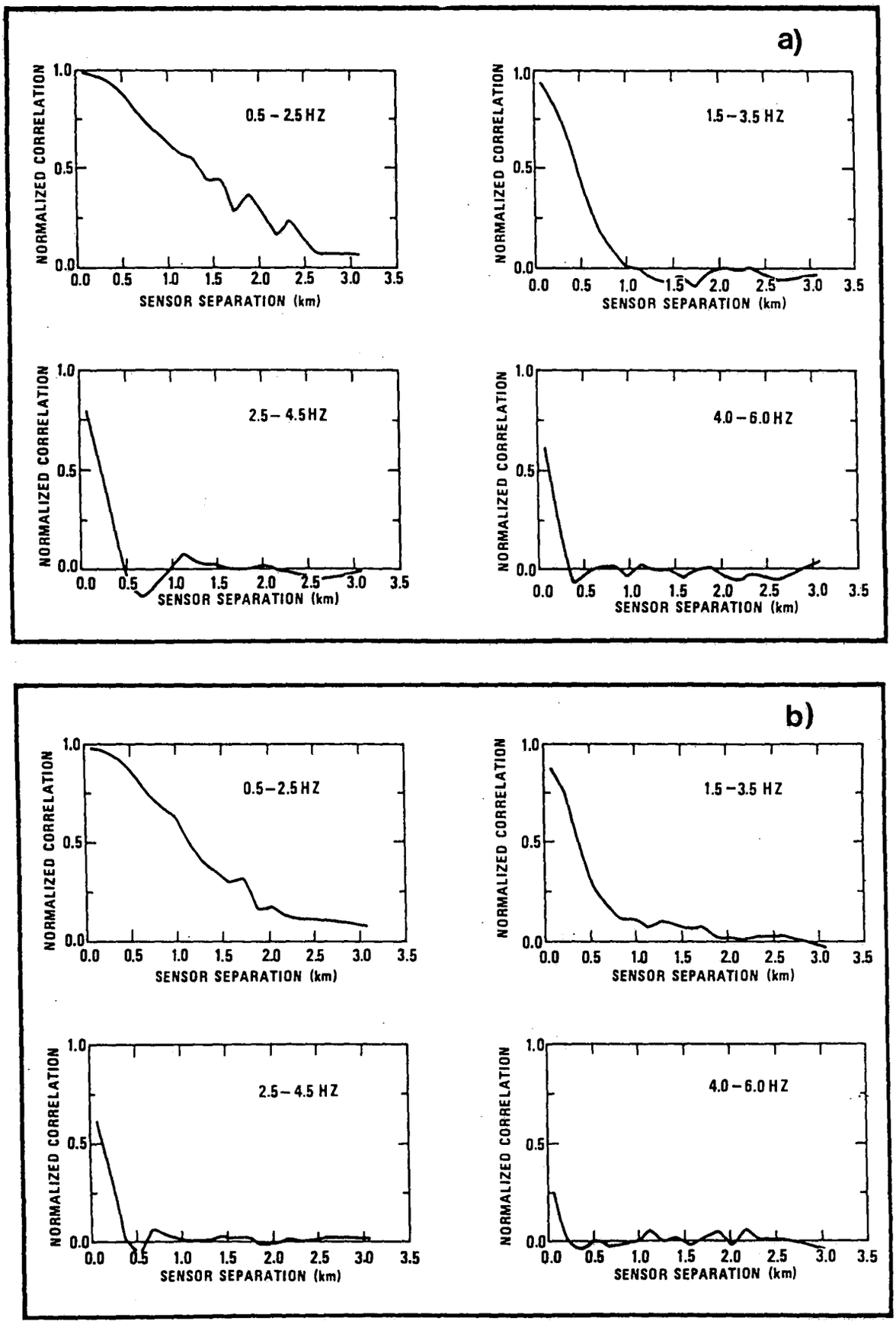

Fig. VII.4.3 Mean normalized correlation curves for noise on the NORESS array as a function of inter-sensor spacing and frequency. a) vertical beam lags; b) horizontal beam lags (azimuth = 0^{o}, velocity = 4.2 km/s). Each curve is an average of 100 sec windows sampled every 5 hours for two days.

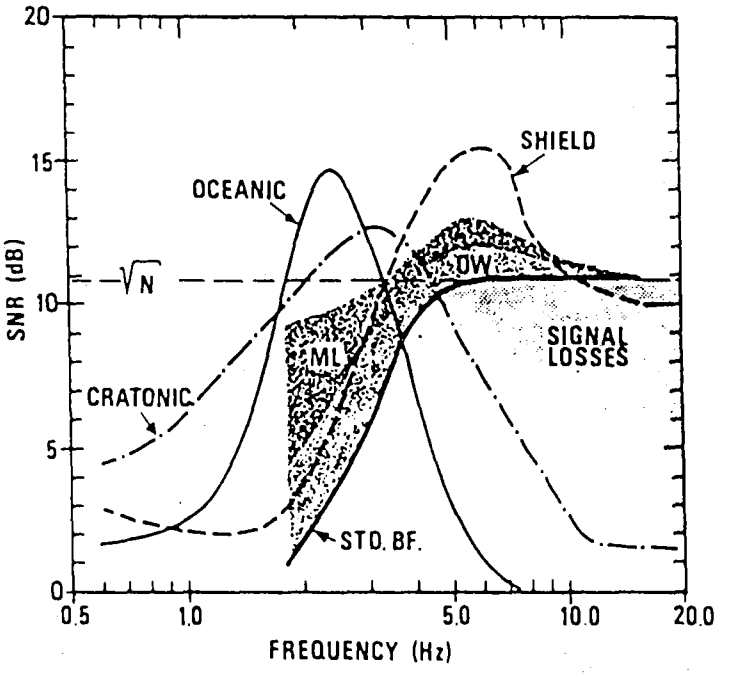

Fig. VII.4.4 SNR-array suppression performance.

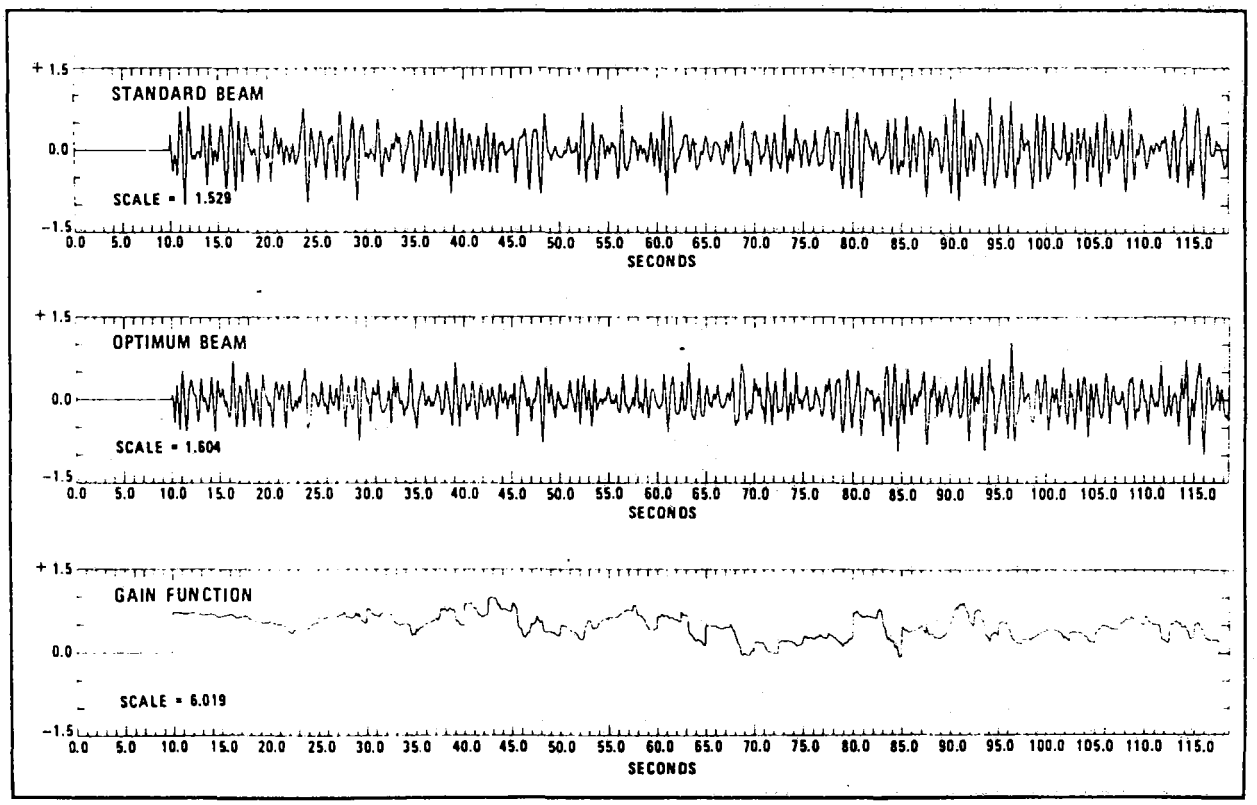

Fig. VII.4.5 Display of standard and optimum beam traces formed during the processing of noise recorded by NORESS. The corresponding gain function is not smooth, but rather fluctuates rapidly in certain time intervals which reflects a degree of non-stationarity in the ambient noise field. The first 10 seconds of data was used to stabilize the covariance matrix, and consequently, not included in the processing. Amplitude scales for the beam traces are in amplitude units, while the amplitude scale for the gain function is in dB.

VII.5 High-frequency P wave attenuation from Central Asia to Norway

It has long been known that the P waves recorded in northern Europe from earthquakes and explosions in Eurasia are often quite rich in high-frequency energy. A detailed quantification of signal transmission characteristics is then possible by studying the spectral characteristics over a broad frequency band. In this study the spectra of NORSAR recordings of some E. Kazakh events are used to develop a model for the average Q along this path. Since the epicentral distance is about 4200 km, this average Q is for paths that penetrate the earth to a depth of about 900 km. The data were processed with the technique applied by Bache et al (1984). For each seismogram energy density spectra are computed for very short (typically 2.2 to 2.5 seconds) time windows isolating the first arriving compressional wave, and the power spectrum of a noise window just before the signal is subtracted. Event spectra are then obtained by averaging over several elements of the array as well as similar events in a small source region, and the spectra obtained this way are quite smooth and are almost entirely shaped by the average source spectrum and the effect of attenuation along the path. Accurate attenuation estimates depend on accurate corrections for the source, assuming that the source spectrum for the direct P wave should be roughly constant up to some corner frequency, above which it is proportional to f^{-n}. For explosions, most of the evidence supports n = 2, and the NORSAR results appear to confirm that value.

The spectra computed from five 8 Hz seismometers for two large Degelen events are shown in Fig. VII.5.1. Also shown is the noise spectrum computed from the average noise power (based on a 3.8 second sample of noise before the signal on each element). The signal spectrum is essentially flat from 3 to beyond 7 Hz when plotted with the f^2 source correction, and the spectra for the other events look much the same.

This is an extraordinary result, as the attenuation has almost no frequency-dependent effect between 3 and 7 Hz. Since attenuation cannot be negative, spectra like this confirm the assumption that the source is proportional to f^{-2} above the corner frequency.

In Fig. VII.V.2 we show the spectra for 6 other events. Four are smaller than the Degelen explosions and two are explosions in other paths of the E. Kazakh test site. The spectra for the Degelen events are all similar to those in Fig. VII.V.2, except that they have the different low-frequency behavior expected for smaller (i.e., higher corner frequency) events. The maximum signal/noise occurs around 7 Hz and decreases at higher frequencies. The events in the other two areas seem to depart from the pattern in that the signal spectrum does not decay so obviously above 7-8 Hz.

Three major features of these spectra determine the attenuation model for the E. Kazakh-NORSAR path. First, at low frequencies they are influenced by source corner frequency effects and a correction for them must be introduced. Second, the source-corrected spectra are essentially flat in the band between 3 and 7 Hz. Finally, the spectra decrease above 7-8 Hz, and we see in Fig. VII.5.3 that the line representing $t^* = 0.14$ is a reasonable approximation for the rate of decay.

For frequencies up to 7 Hz, the attenuation effects can be represented by an absorption band model. This is best done with a "path average" spectrum obtained by averaging several spectra (here six), as shown in Fig. VII.5.4, obtaining a spectrum which essentially is a smoothed version of the single event spectra in Fig. VII.5.1. In Fig. VII.5.4 we also show an estimate for the spectrum after correcting for source corner frequency effects and the spectra for several attenuation models. The corner frequency correction is based on spectra computed by Bache et al (1984), utilizing the spectral difference between Dege-

len and low corner frequency Shagan events to approximately correct the Degelen spectra. A roughly "corrected" spectrum (Fig. VII.5.4) shows that the slope changes below 3 Hz, even though this "corrected" spectrum still underestimates attenuation effects at low frequency.

In Fig. VII.5.4 the "corrected" NORSAR spectrum is plotted with the spectral effect of several absorption band models (Minster, 1978). For this application the model has two parameters, t_o^*, which is the ratio of travel time to average path Q at long periods, and τ_m, which specifies where the Q^{-1} begins to decrease with frequency. The key spectral features are the frequency dependence below 3 Hz and the nearly horizontal slope up to 7 Hz. The best fit seems to be with models having $t_o^* \simeq 0.6$ seconds (not much constrained by these data) and τ_m slightly greater than 0.05 seconds. For such models the effect of attenuation above 3 Hz reduces to multiplication of the spectrum by a constant, which is about 0.04 for $t_o^* = 0.6$, $\tau_m = 0.06$; and 0.07 for $t_o^* = 0.5$, $\tau_m = 0.06$. Obviously, the value of this constant depends on the choice of t_o^*, characterized by the attenuation at long periods.

An absorption band model with $0.05 < \tau_m < 0.1$ and $t_o^* \simeq 0.6$ was found by Bache et al (1984) to represent the low frequency attenuation on the paths from eastern Kazakhstan to four UKAEA arrays, with frequencies above 3 Hz, requiring a second Q^{-1} to explain the constant rate of spectral decay seen at those frequencies. In view of Figs. VII.5.2 VII.5.3, the NORSAR path data also require a second Q superimposed on the absorption band model, but its effect is not felt until 7 Hz and beyond. Thus, similar two-part Q models seem to fit the data for all five paths (with minor adjustments in the t_o^* and τ_m), with the major difference being that the effect of the second Q is not felt until higher frequencies at NORSAR.

A key feature of the NORSAR spectra is thus that the effect of attenuation is little more than multiplication by a constant for frequen-

cies between 3 and 7 Hz. Physical mechanisms for absorption must be characterized by $Q \approx f$ above some high-frequency limit on the relaxation spectrum, so absorption band models (e.g., Anderson and Given, 1982) anticipate that attenuation must reduce to a constant multiplier above some limiting frequency. These NORSAR spectra provide an unambiguous observation that such behavior does indeed exist. For most paths it is difficult to observe apparently because attenuation by scattering masks it.

It is not known whether or not the E. Kazakh-NORSAR path is typical of the Eurasian continent. If it is, the detection capability of systems to monitor nuclear explosion testing in this region could be much improved by greater emphasis on high-frequency data. An estimate of the anticipated improvement was recently made by Evernden et al (1984), but it should be noted that these authors made much more optimistic assumptions about the signal/noise at high frequencies than can be supported by the NORSAR data presented here. Some improvement of the NORSAR signal/noise at high frequencies may be possible by using arrays designed specifically for this purpose (e.g., Mykkeltveit et al, 1983), but the scattering attenuation may be impossible to overcome since it is probably due to inhomogeneous structure throughout the lithosphere. Regional phases like P_n also seem likely to be attenuated by scattering at high frequencies. While better use of high-frequency data may improve detection, this is far easier than identifying an event, and more work remains to be done until one knows how much the capability for improving event identification can be improved by exploiting these high-frequency data.

More details about the research reported on here are given in Bache and Bungum (1984).

T.C. Bache (Science Applications International, La Jolla)
H. Bungum

References

Anderson, D.L. and J.W. Given (1982). Absorption band Q model for the earth, J. Geophys. Res. 81, 3983-3904.

Bache, T.C. and H. Bungum (1984). High-frequency P wave attenuation from Central Asia. Submitted to Geophys. J. R. astr. Soc.

Bache, T.C., P.D. Marshall and L.B. Bache (1984). Q for teleseismic P waves from Central Asia. Submitted for publication to J. Geophys. Res.

Evernden, J.F., C.B. Archambeau and E. Cranswick (1984). An updated evaluation of seismic decoupling (in preparation).

Minster, J.B. (1978). Transient and impulse responses of a one-dimensional linearly attenuating medium - II. A parametric study. Geophys. J. R. astron. Soc. 52, 503-524.

Mykkeltveit, S., K. Åstebøl, D.J. Doornbos and E.S. Husebye (1983). Seismic array configuration optimization, Bull. Seism. Soc. Am. 73, 173-186.

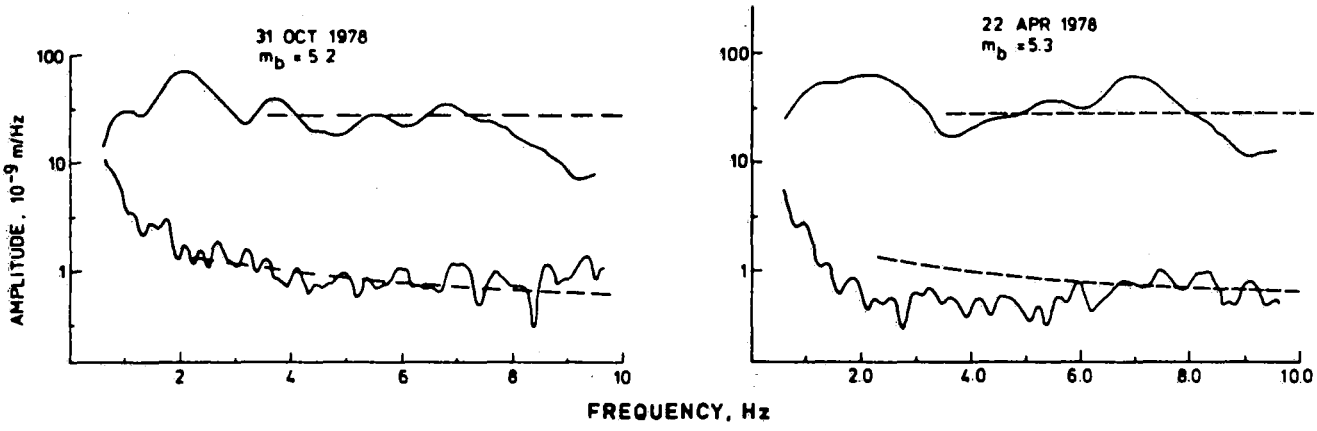

Fig. VII.5.1 The spectra for two of the events of (Table 2 ?) are shown together with the average noise window just before the P signal. A horizontal dashed line is sketched through each signal spectrum and the NORSAR noise model of Bungum (1983) is sketched through the noise.

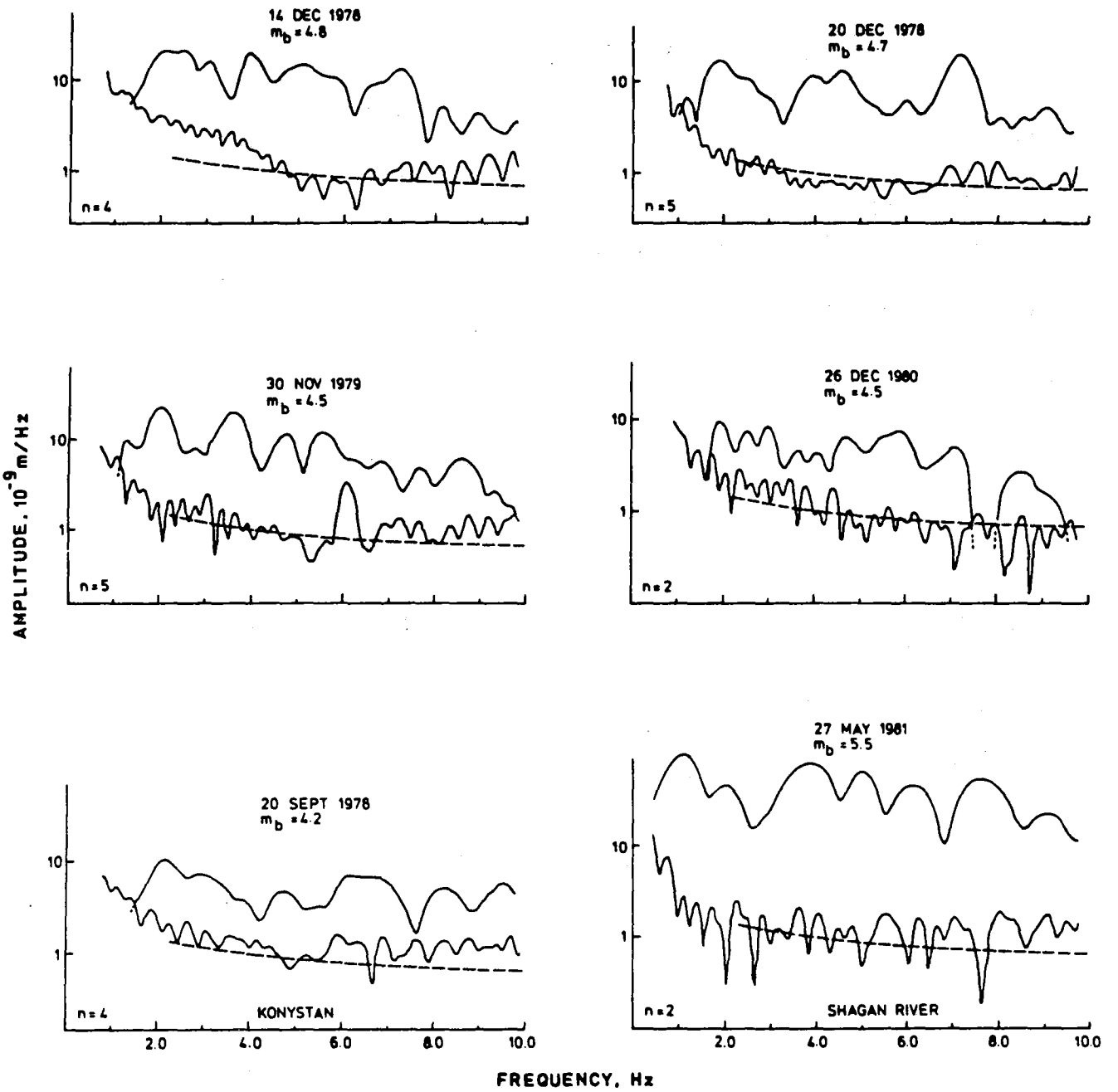

Fig. VII.5.2 Spectra are plotted for six events in the same format as Fig. VII.5.1. The number of elements included in the spectrum is indicated by n.

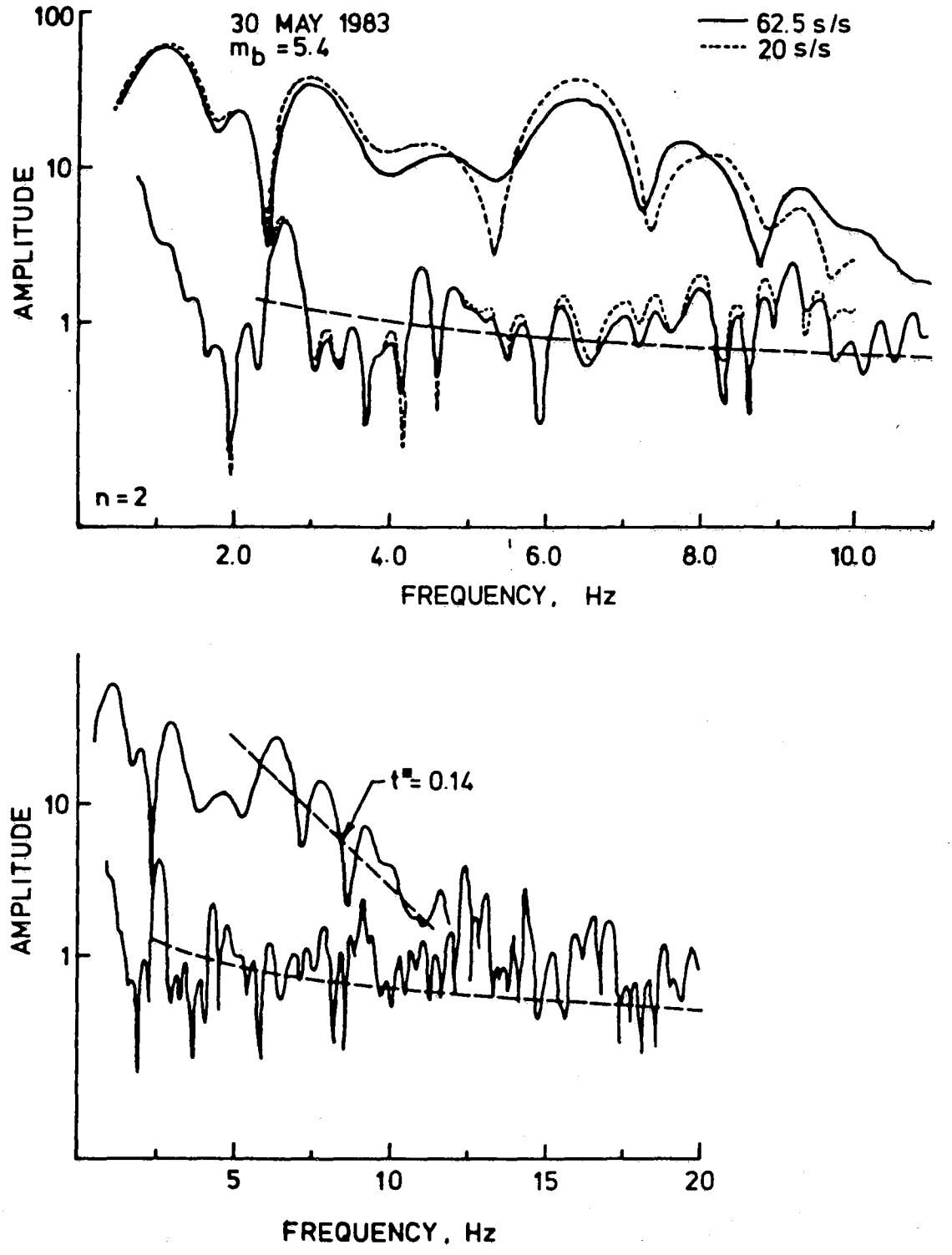

Fig. VII.5.3 Signal and noise spectra are plotted for an event digitized at two different sampling rates. The higher sampling rate spectra are then replotted on a different frequency scale (bottom). On the latter a line with a slope corresponding to t* = 0.14 is drawn through the high-frequency portion of the signal spectrum.

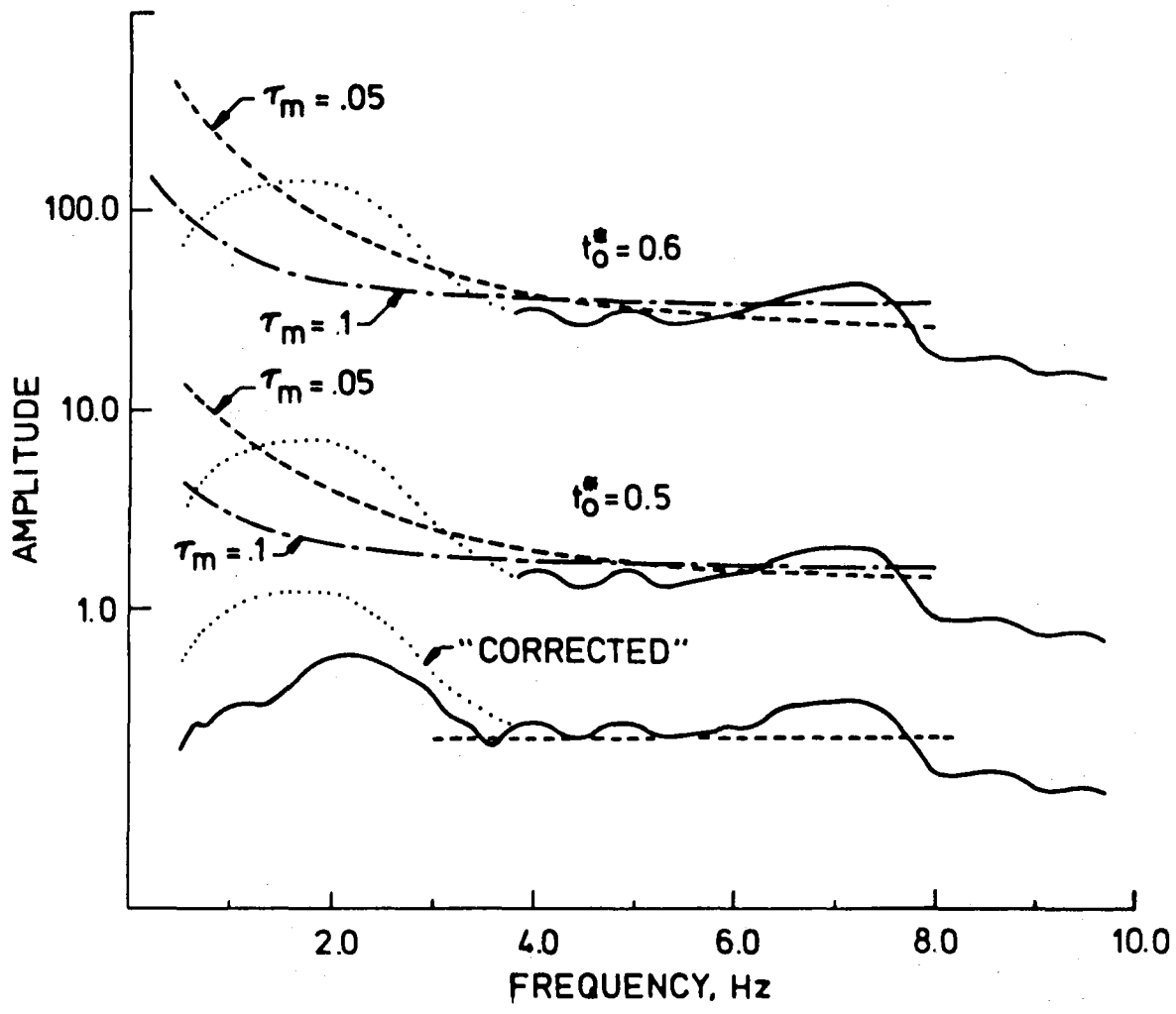

Fig. VII.5.4 The bottom sketch shows the path average spectrum together with a horizontal line and a dotted line showing this spectrum corrected for corner frequency effects. The top two sketches show this corrected spectrum with the spectral effect of several absorption band models for attenuation.

VII.6 Teleseismic detection at high frequencies using NORSAR data

This paper summarizes initial results from NORSAR noise and signal studies aimed at identifying possibilities to improve the detection capability of the NORSAR array. Particular emphasis is given to high-frequency signals (2-5 Hz), which are typical for NORSAR recordings of many Eurasian events.

Noise characteristics. Bungum and Mykkeltveit (1984) have summarized the main features of seismic noise spectra observed at NORSAR. These spectra are characterized by a very strong microseismic peak at 0.2-0.3 Hz, especially during North Sea storm activity. The spectral slope is very steep (50 dB/decade) up to at least 40 Hz, and the NORSAR noise at high frequencies is among the lowest observed. Above 2 Hz, there is little difference between "high noise" and "low noise" conditions, except that cultural activities cause increases in high frequency noise during day time. Because of the limited resolution and gain ranging applied at NORSAR, the spectra actually observed at NORSAR instruments are biased high above 3 Hz as discussed by Bungum (1983).

Signal characteristics. Main features, discussed by Ringdal and Husebye (1982) are a) large and region-dependent variation in signal levels across NORSAR, often spanning an order of magnitude across the array, b) significant deviations from a plane wavefront model, making steering delay corrections necessary in the beamforming process, and c) significant energy at high frequencies (> 2 Hz) from Eurasia, especially for underground explosions.

Detection algorithms. Current Detection Processor (DP) procedure at NORSAR (Ringdal, 1981) is to form conventional array beams with a filter of 1.2-3.2 Hz and envelope beams with a filter of 1.6-3.2 Hz. These beams are then subjected to a linear STA/LTA detector and passed

through a grouping algorithm to delete side lobe detections. In the present study, we have analyzed SNR of a number of presumed explosions from Eurasia by applying 8 predetermined bandpass filters to:

(a) An array beam using current DP steering delays (0.1 sec accuracy)
(b) An array beam using recomputed delays (0.05 sec accuracy)
(c) An optimum weighted array beam, with steering delays as in (b) and each channel weighted by S/N^2 (S = signal amplitude, N = noise amplitude)
(d) The best subarray beam for the particular event.

Examples of results are shown for two events in Figs. VII.6.1 and VII.6.2. These results, which are largely confirmed (with few exceptions) by the other events analyzed, give that:

(a) Significant gains are possible by applying more high-frequent filters than currently done.
(b) The weighted array beam is generally best, while the best subarray beam SNR is quite close (within 2-3 dB average).
(c) Gains compared to current processing can reach 10-20 dB for high-frequent signals, and somewhat less for signals of low dominant frequency.

Detection performance for presumed explosions. By comparing the SNR of the best beam to the event magnitude, it is possible to estimate approximately the optimum NORSAR thresholds, i.e., thresholds that could be achieved if processing as indicated above were implemented. We have found that (cf. Figs. VII.6.3 and VII.6.4) these "instantaneous" detection thresholds are:

- West of Ural Mountains: m_b 2.0-2.5 (possibly better)
- Caspian Area m_b 2.0-2.5
- Semipalatinsk m_b 2.5-3.0
- Siberia m_b 2.5-3.5

It is noteworthy that there is a large range in thresholds across Eurasia, and this can be interpreted as being due to "source focusing" effects similar to the "receiver focusing" effects routinely observed at NORSAR.

Detection in the coda of an earthquake. An example of the importance of high-frequency detection in this connection is given in Fig. VII.6.5, where NORSAR 06C06 signals from an m_b 5.8 earthquake near Kamchatka are followed one minute later by signals from a presumed explosion (m_b 3.8) at Semipalatinsk. With the standard 1.2-3.2 Hz filter, the latter signal is completely masked by the coda, whereas a filter of 3.2-5.2 Hz shows the explosion signal dominating that of the earthquake. This figure is based on a single instrument, and further improvements are of course possible by multichannel processing.

In conclusion, the demonstrated gains from high-frequency processing of teleseismic explosions clearly warrant a modification in the present NORSAR detection algorithms. The practical implementation of these changes is now the subject of further study.

F. Ringdal

References

Bungum, H. (1983). Power spectral bias sources and quantization levels, in Semiannual Technical Summary 1 Oct 82 - 31 Mar 83, NORSAR Sci. Rep. 2-82/83.

Bungum, H. & S. Mykkeltveit (1984). Seismic noise at high-frequencies, to be published.

Ringdal, F. (1981). Automatic processing methods in the analysis of data from a global seismic network, in NATO ASI Proceedings, Identification of Seismic Sources, D. Reidel Publ. Co.

Ringdal, F. & E.S. Husebye (1982). Application of arrays in the detection, location and identification of seismic events, Bull. Seism. Soc. Am. 72, S201-S224.

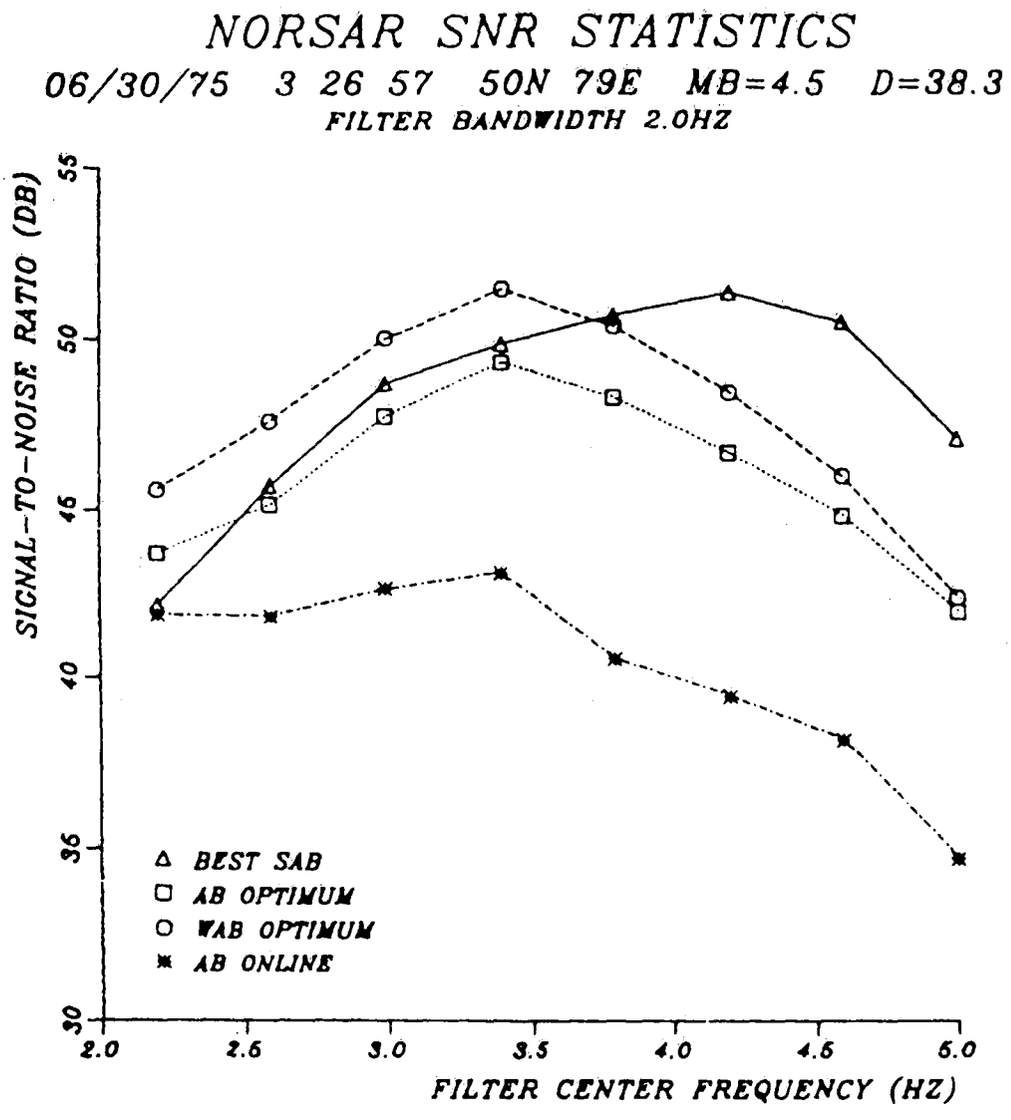

Fig. VII.6.1 Observed SNR at NORSAR for different filters and beam-forming methods, as explained in the text. The case shown is an m_b 4.5 Semipalatinsk presumed explosion.

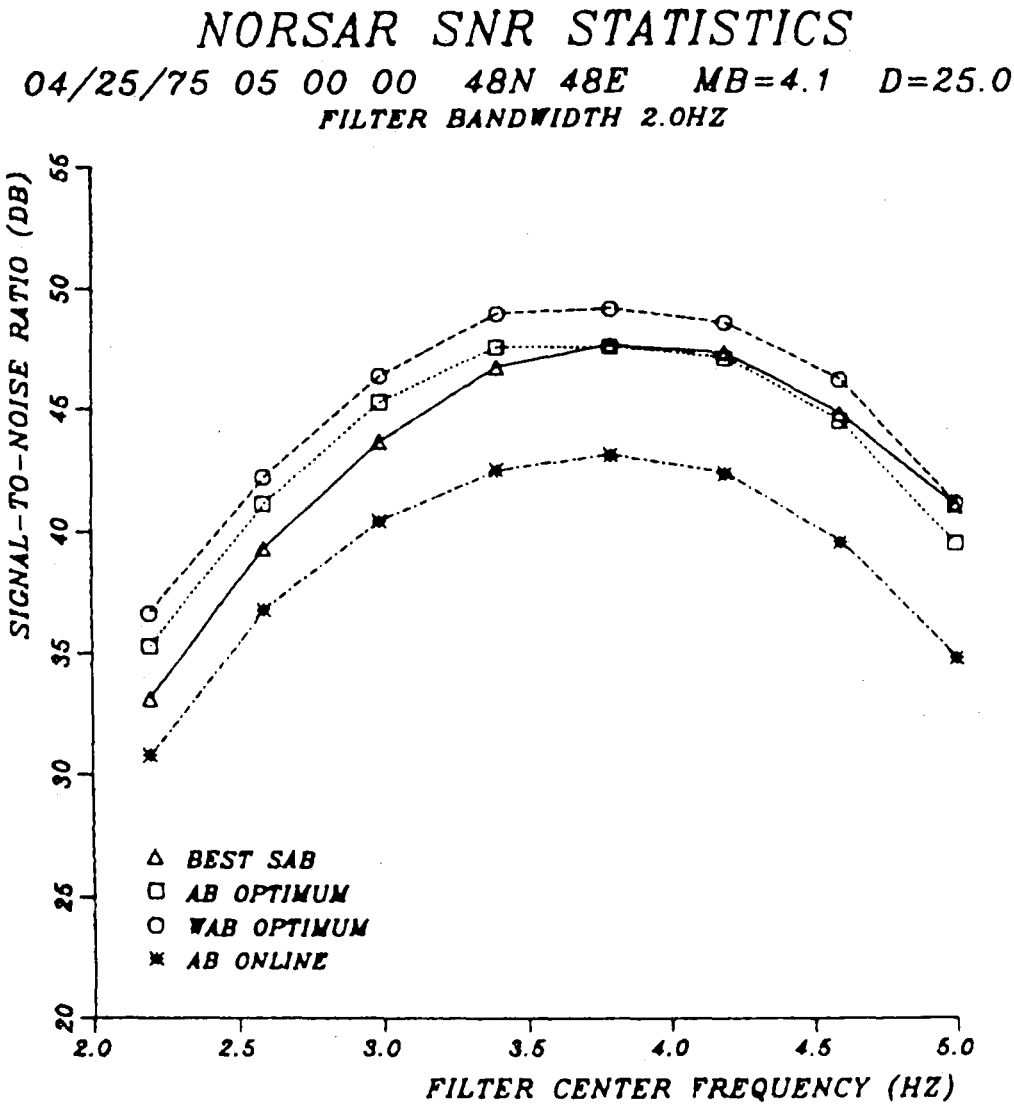

Fig.VII.6.2 Same as Fig. VII.6.1, but for a presumed explosion from the Azgir area.

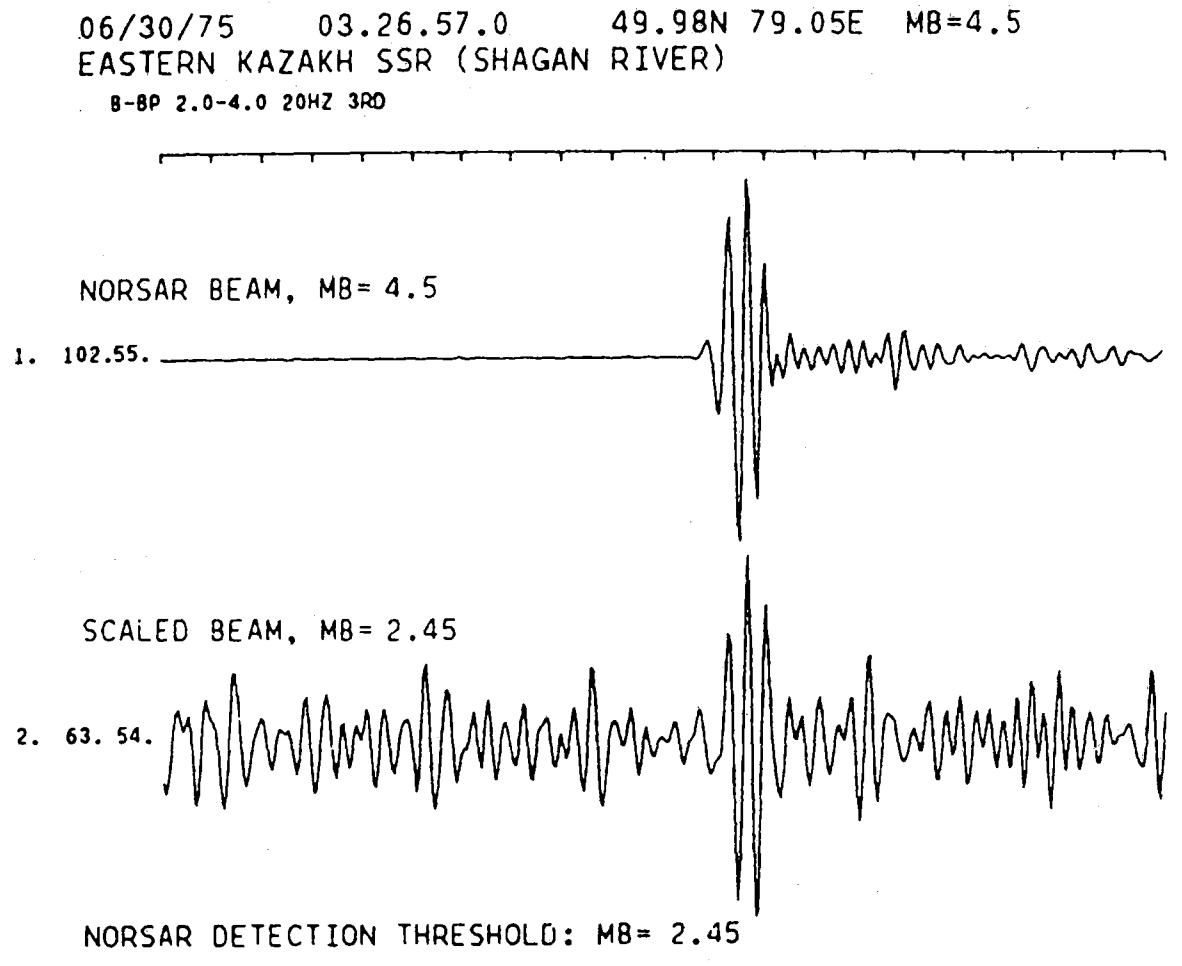

Fig. VII.6.3 NORSAR array beam (top) and a scaled beam added to preceding noise, and indicating the "optimum" instantaneous dectection threshold. This figure corresponds to the event of Fig. VII.6.1. Note that this is a "best case" event, and that typical scaled thresholds for other Semipalatinsk events range from m_b 2.5 to 3.0.

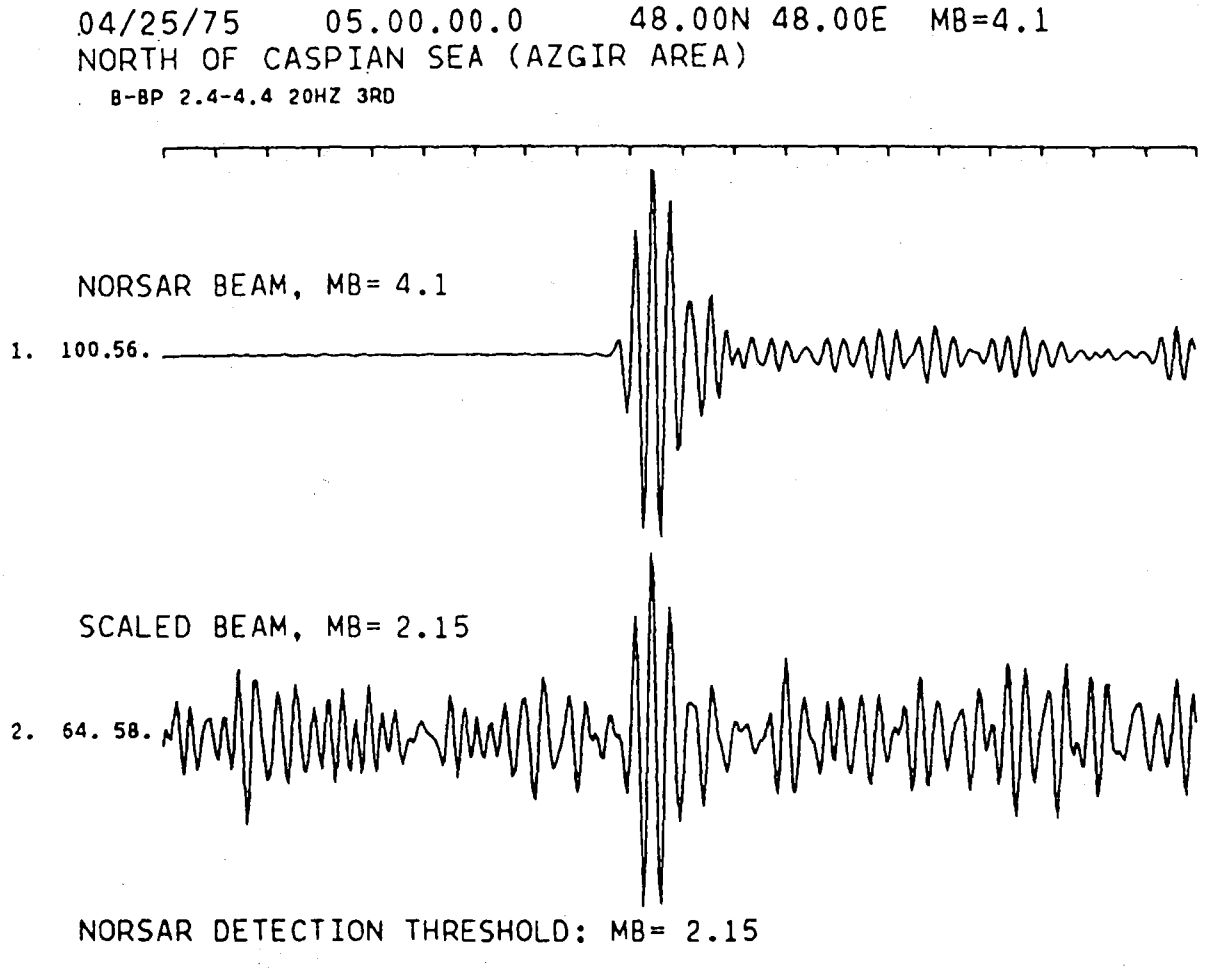

Fig. VII.6.4 Same as Fig. VII.6.3, but corresponding to the event of Fig. VII.6.2. Other events studied from this area have given scaled thresholds from m_b 2.2 to 2.5.

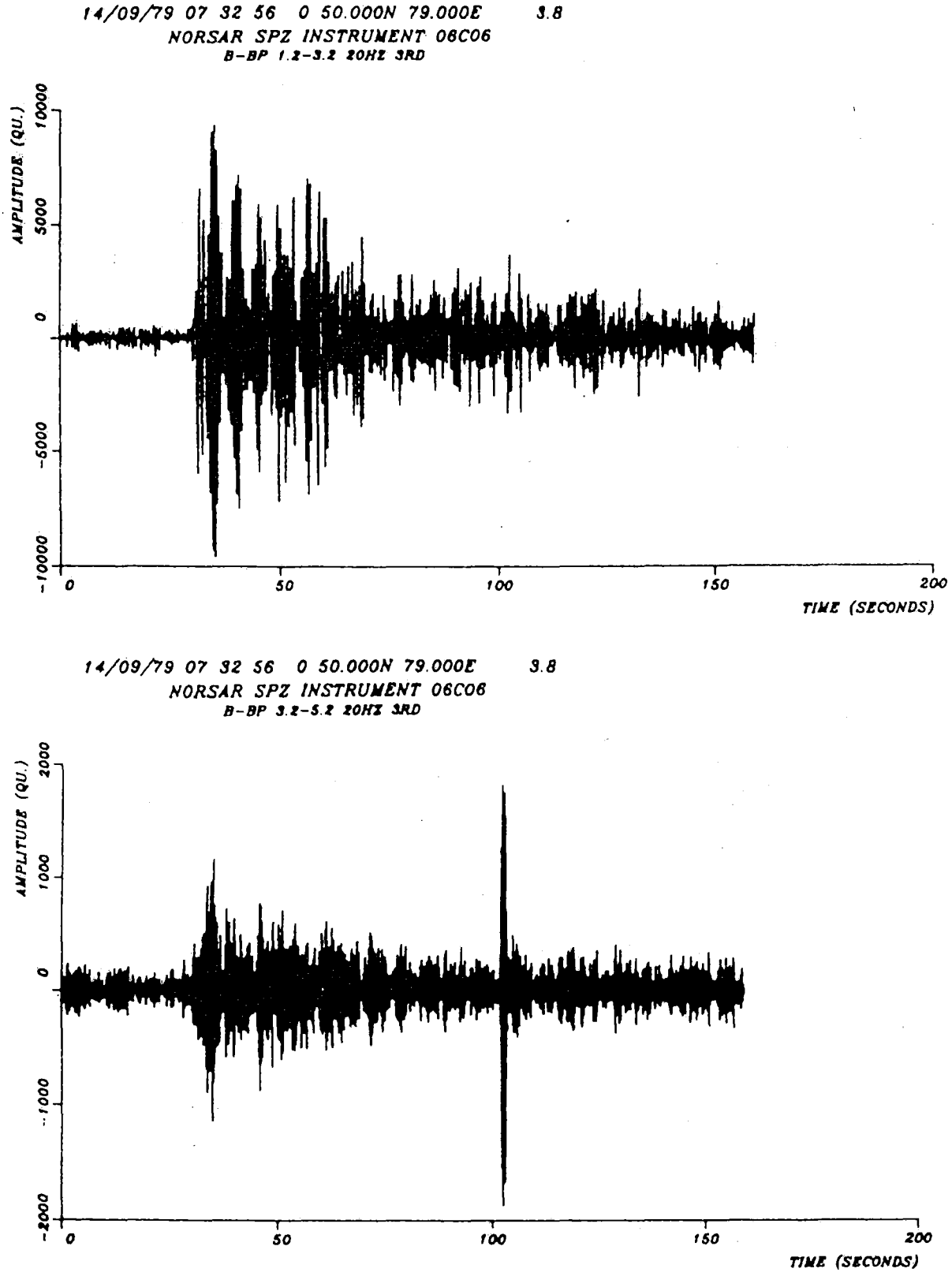

Fig. VII.6.5 Example of NORSAR recordings instrument 06C06 from a small presumed explosion with signal arrival one minute later than that of a preceding large earthquake. Note that the explosion signal is not visible on the top trace (1.2-3.2 Hz filter), but can be clearly seen on the bottom trace (3.2-5.2 Hz filter).

VII.7.1 NORESS Regional Array developments

Evaluation of the performance of the newly established NORESS array in Norway has been initiated. In particular, real time processing algorithms aimed at detection and location of events at regional distances have been developed and tested.

The design criteria and associated specifications on the performance of the new array were originally formulated as follows:

- Detection: The array should provide optimum SNR gain by beamforming.
- Location: The array should have a narrow main lobe and small side lobes.
- Performance as a function of signal frequency: The array performance should be good or at least reasonable for a wide range of frequencies, typical of regional wave propagation.
- Research aspects: The array should have an optimum coarray pattern. Add as many horizontal component seismometers as can be afforded (within the geometry of the vertical array).

The array geometry of Fig.VII.7.1 was worked out in close cooperation between Sandia, LLNL and NORSAR. It represents the best compromise we found between the partly conflicting demands made above on array performance. In the design work, we were able to draw heavily on the experience gained from several provisional array installations in Norway. For example, actually observed correlations for signals and noise were used to optimize the SNR gain. For evaluation of the location capability of the new array, beam patterns were computed for realistic signal correlations. The geometry of Fig. VII.7.1 contains useful subgeometries, which are close to optimum for different frequencies within the range 2-10 Hz.

In order to have an experimental check on the proposed geometry, a provisional 21-element array was installed during the summer of 1983. Analysis of data from this installation has confirmed the correlation

curves for signals and noise on which the design work was based. Testing of the RONAPP processing package (Mykkeltveit & Bungum, 1984) for regional events recorded on this array, shows that the arrival azimuths can be estimated to within a few degrees of the true value.

Results from the 1983 provisional installation basically confirmed the projected capabilities of the new array, and it was finally decided to deploy an array with the geometry given in Fig. VII.7.1.

The final array installed during the summer of 1984 comprises 25 short period elements, 4 out of which are 3-axis deployments with the remaining 21 elements consisting of vertical-motion seismometers only. In addition, there is a broad-band 3-axis system. Sampling rates are 40 Hz for the short period channels and 10 Hz (intermediate period) and 1 Hz (long period) for the broadband system. Data from the new array are transmitted to Kjeller via a leased land line and via satellite to the U.S. Preliminary analysis of the new data has given promising results. Fig. VII.7.2 gives an example of the automatic output from the on-line event processing of data from the new array.

Several improvements to the on-line processing package are under way. For instance, the success of the location part of the RONAPP processing package depends on a proper identification of the secondary phase associated with the P arrival. This secondary phase is either Lg or Sn and a priori knowledge on the occurrence of these phases on the NORESS records as a function of source region will be incorporated in RONAPP. For this end, regional data recorded at NORSAR over the past 13 years have been examined. The general picture is that Lg is the dominant secondary arrival, but notable exceptions have been identified, corresponding to source regions for which Sn is the more prominent or even sole secondary phase. Fig. VII.7.3 gives an example of

a tectonic feature in the North Sea that is an effective barrier to Lg wave propagation (Kennett & Mykkeltveit, 1984).

S. Mykkeltveit

References

Kennett, B.L.N. & S. Mykkeltveit (1984). Guided wave propagation in laterally varying media - II. Lg waves in north-western Europe.

Mykkeltveit, S. & H. Bungum (1984). Processing of regional seismic events using data from small-aperture arrays. Bull. Seism. Soc. Am., December 1984.

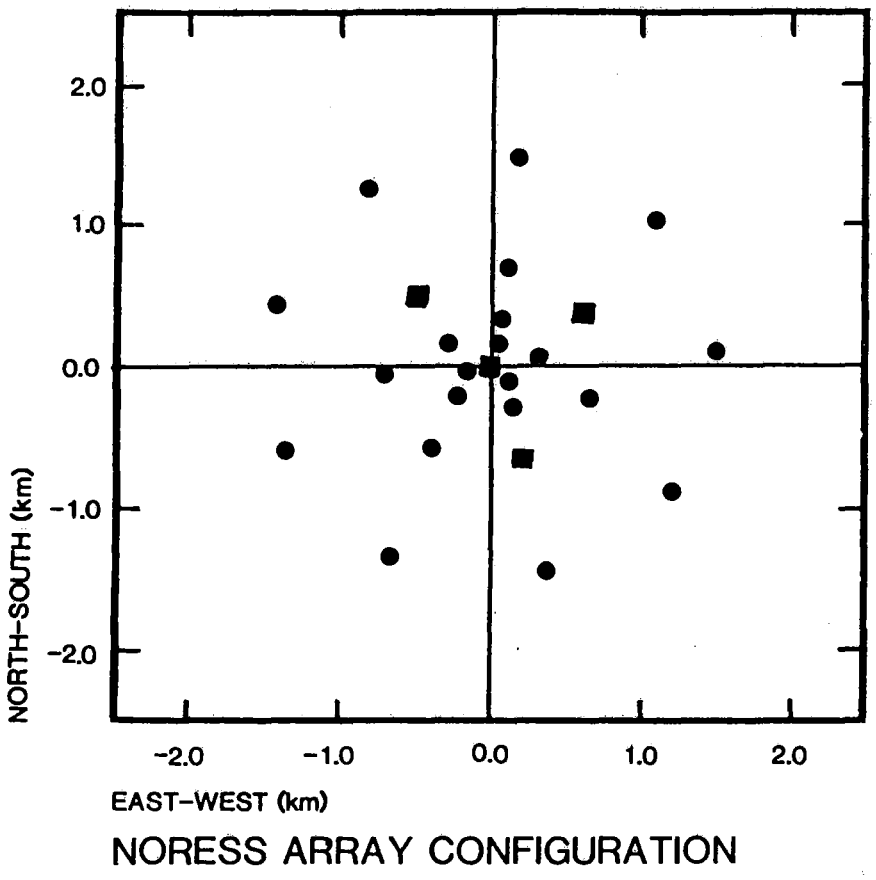

Fig. VII.7.1 Geometry of the new NORESS array, which has been installed during the summer of 1984. The four three-axis instruments are indicated by squares. All instruments are in shallow vaults, except the three-axis seismometer at the center of the array, which is installed in a 60 m deep borhole.

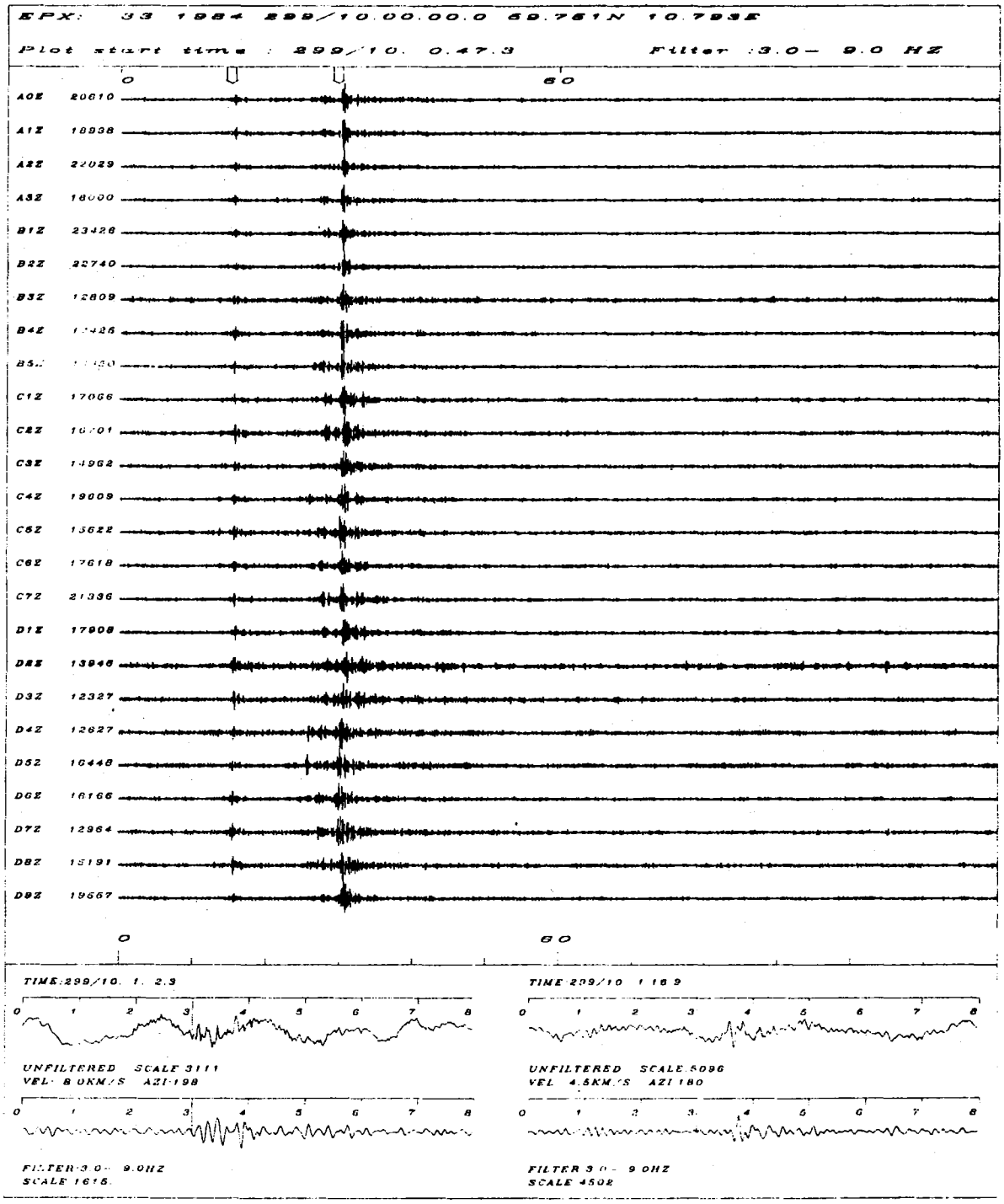

Fig. VII.7.2a Vertical component records from the new NORESS array for a local event detected and located by RONAPP. The two arrivals detected and associated are marked by arrows. Bottom: Unfiltered and filtered beams for the two detections.

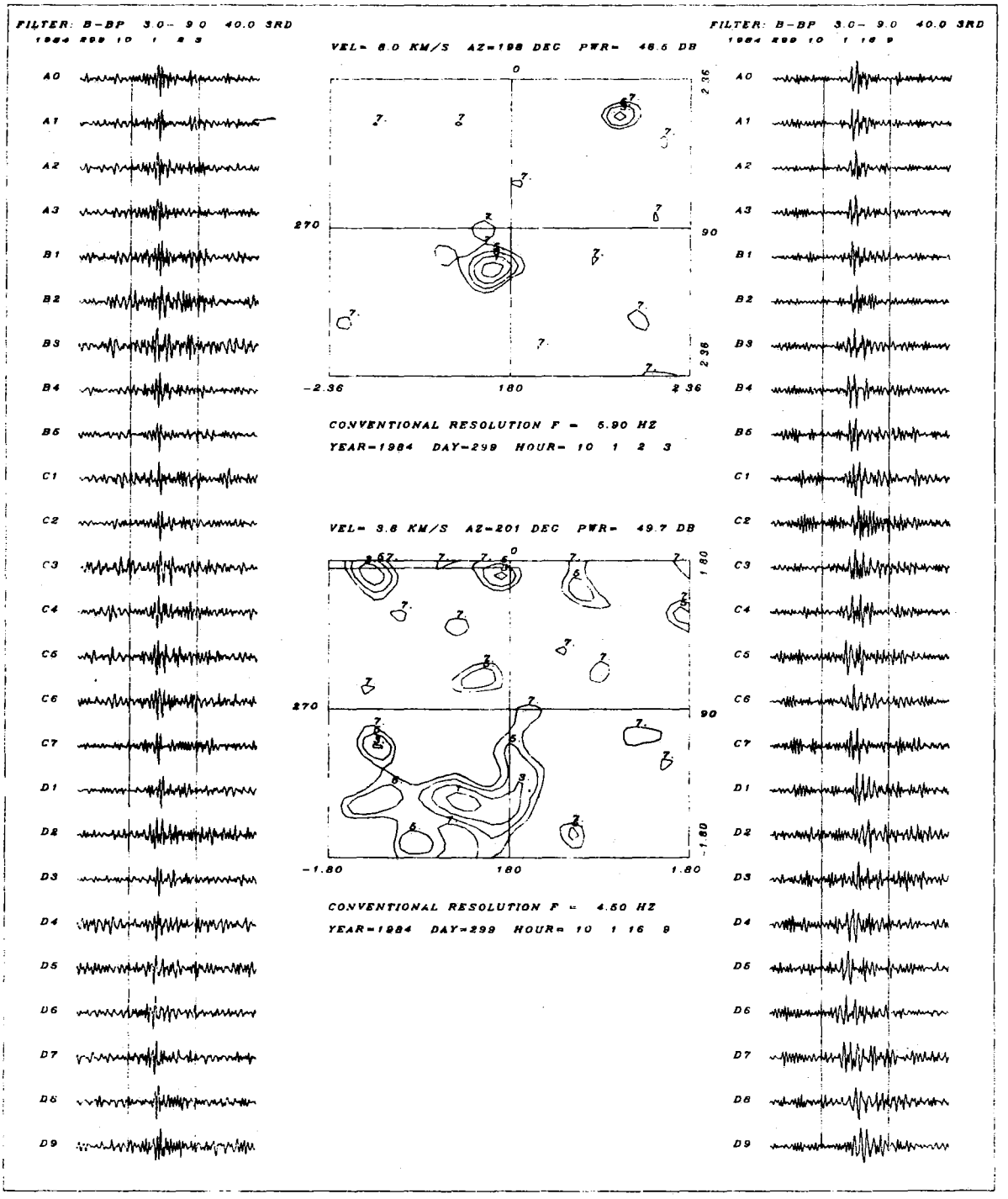

Fig. VII.7.2b Results of frequency-wavenumber analysis of the indicated time windows around the two detections in Fig. VII.7.2a.

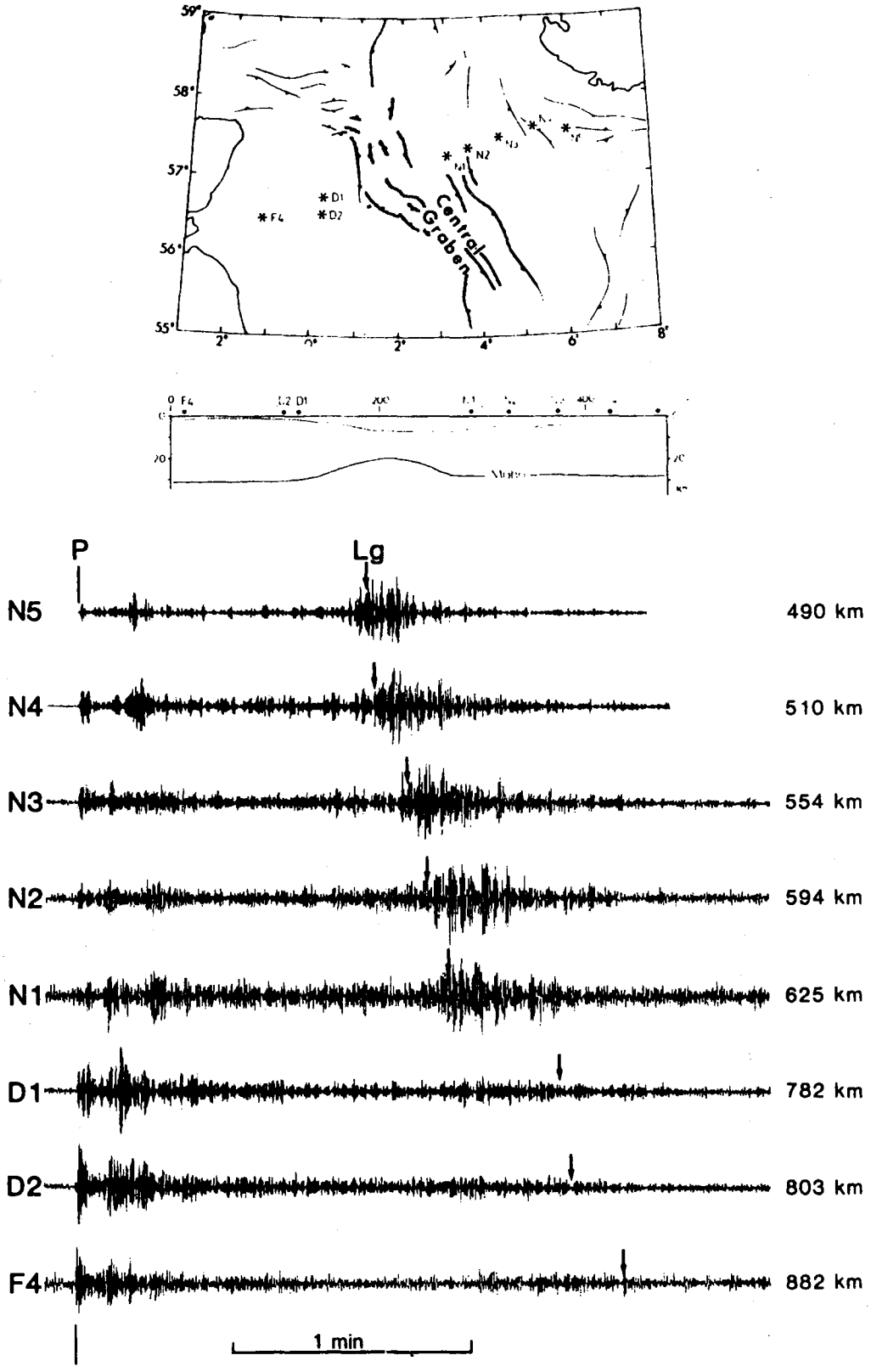

Fig. VII.7.3 Map of the central North Sea Basin (top) and main structural features (middle). NORSAR records from shots located at positions indicated in the map. Arrows indicate a group velocity of 3.5 kms^{-1} corresponding to Lg wave arrivals.